



**UNIVERSIDAD DE INVESTIGACIÓN DE TECNOLOGÍA  
EXPERIMENTAL YACHAY**

**Escuela de Ciencias Físicas y Nanotecnología**

**TÍTULO: Tunneling through a Spin Barrier in Chiral Molecules**

Trabajo de integración curricular presentado como requisito para la  
obtención  
del título de Físico

**Autor:**

Zambrano García Iskra Nicole

**Tutor:**

Ph.D. Medina Dagger Ernesto Antonio

Urcuquí, Diciembre 2020

Urcuquí, 10 de noviembre de 2020

**SECRETARÍA GENERAL**  
**(Vicerrectorado Académico/Cancillería)**  
**ESCUELA DE CIENCIAS FÍSICAS Y NANOTECNOLOGÍA**  
**CARRERA DE FÍSICA**  
**ACTA DE DEFENSA No. UITEY-PHY-2020-00021-AD**

A los 10 días del mes de noviembre de 2020, a las 11:40 horas, de manera virtual mediante videoconferencia, y ante el Tribunal Calificador, integrado por los docentes:

<b>Presidente Tribunal de Defensa</b>	Dr. CHACON TORRES, JULIO CESAR , Ph.D.
<b>Miembro No Tutor</b>	Dr. ZAMORA LEDEZMA , CAMILO , Ph.D.
<b>Tutor</b>	Dr. MEDINA DAGGER, ERNESTO ANTONIO, Ph.D.

El(la) señor(ita) estudiante **ZAMBRANO GARCIA, ISKRA NICOLE**, con cédula de identidad No. **0803740497**, de la **ESCUELA DE CIENCIAS FÍSICAS Y NANOTECNOLOGÍA**, de la Carrera de **FÍSICA**, aprobada por el Consejo de Educación Superior (CES), mediante Resolución **RPC-SO-39-No.456-2014**, realiza a través de videoconferencia, la sustentación de su trabajo de titulación denominado: **TUNNELING THROUGH A SPIN ACTIVE BARRIER IN CHIRAL MOLECULES**, previa a la obtención del título de **FÍSICO/A**.

El citado trabajo de titulación, fue debidamente aprobado por el(los) docente(s):

<b>Tutor</b>	Dr. MEDINA DAGGER, ERNESTO ANTONIO, Ph.D.
--------------	---

Y recibió las observaciones de los otros miembros del Tribunal Calificador, las mismas que han sido incorporadas por el(la) estudiante.

Previamente cumplidos los requisitos legales y reglamentarios, el trabajo de titulación fue sustentado por el(la) estudiante y examinado por los miembros del Tribunal Calificador. Escuchada la sustentación del trabajo de titulación a través de videoconferencia, que integró la exposición de el(la) estudiante sobre el contenido de la misma y las preguntas formuladas por los miembros del Tribunal, se califica la sustentación del trabajo de titulación con las siguientes calificaciones:

Tipo	Docente	Calificación
Miembro Tribunal De Defensa	Dr. ZAMORA LEDEZMA , CAMILO , Ph.D.	9,9
Tutor	Dr. MEDINA DAGGER, ERNESTO ANTONIO, Ph.D.	8,9
Presidente Tribunal De Defensa	Dr. CHACON TORRES, JULIO CESAR , Ph.D.	9,7

Lo que da un promedio de: **9.5 (Nueve punto Cinco)**, sobre 10 (diez), equivalente a: **APROBADO**

Para constancia de lo actuado, firman los miembros del Tribunal Calificador, el/la estudiante y el/la secretario ad-hoc.

Certifico que *en cumplimiento del Decreto Ejecutivo 1017 de 16 de marzo de 2020, la defensa de trabajo de titulación (o examen de grado modalidad teórico práctica) se realizó vía virtual, por lo que las firmas de los miembros del Tribunal de Defensa de Grado, constan en forma digital.*

ZAMBRANO GARCIA, ISKRA NICOLE  
**Estudiante**



Dr. CHACON TORRES, JULIO CESAR , Ph.D.  
**Presidente Tribunal de Defensa**



Dr. MEDINA DAGGER, ERNESTO ANTONIO, Ph.D.  
**Tutor**



Firmado electrónicamente por:  
**ERNESTO ANTONIO**  
**MEDINA DAGGER**

CAMILO  
ZAMORA  
LEDEZMA

Firmado digitalmente por  
CAMILO ZAMORA  
LEDEZMA  
Fecha: 2020.11.19 18:42:40  
-05'00'

Dr. ZAMORA LEDEZMA , CAMILO , Ph.D.  
**Miembro No Tutor**



Firmado electrónicamente por:  
KARLA  
ESTEFANIA  
ALARCON FELIX

ALARCON FELIX, KARLA ESTEFANIA  
**Secretario Ad-hoc**

## AUTORÍA

Yo, **Iskra Nicole Zambrano García**, con cédula de identidad 0803740497, declaro que las ideas, juicios, valoraciones, interpretaciones, consultas bibliográficas, definiciones y conceptualizaciones expuestas en el presente trabajo; así cómo, los procedimientos y herramientas utilizadas en la investigación, son de absoluta responsabilidad de el/la autora (a) del trabajo de integración curricular. Así mismo, me acojo a los reglamentos internos de la Universidad de Investigación de Tecnología Experimental Yachay.

Urcuquí, diciembre 2020.



---

Iskra Nicole Zambrano García  
CI: 0803740497

## AUTORIZACIÓN DE PUBLICACIÓN

Yo, **Iskra Nicole Zambrano García**, con cédula de identidad 0803740497, cedo a la Universidad de Tecnología Experimental Yachay, los derechos de publicación de la presente obra, sin que deba haber un reconocimiento económico por este concepto. Declaro además que el texto del presente trabajo de titulación no podrá ser cedido a ninguna empresa editorial para su publicación u otros fines, sin contar previamente con la autorización escrita de la Universidad.

Asimismo, autorizo a la Universidad que realice la digitalización y publicación de este trabajo de integración curricular en el repositorio virtual, de conformidad a lo dispuesto en el Art. 144 de la Ley Orgánica de Educación Superior

Urcuquí, Diciembre 2020.



---

Iskra Nicole Zambrano García  
CI: 0803740497

## **Dedication**

To my family, especially to my mom and my little son Mateo, who have been my impulse and my happiness during all these years.

Iskra Nicole Zambrano García

## Acknowledgements

I want to express my gratitude to two people who made this achievement possible, my advisor and co-advisor of this work. Many thanks to Dr. Ernesto Medina for believing in me, allowing me to work with him and share his knowledge with me, I have learned a lot from him. An infinite thanks to Dr. Solmar Varela for all the patience and dedication she has had with me, thank you for always motivating and inspiring me and teaching me I can do science and have fun at the same time.

I thank Yachay Tech University for training us as young scientists, I have learned a lot in these years and I am proud to continue on the path of science. Thanks to the School of Physical Sciences and Nanotechnology for opening its doors to me, especially to my professors for transmitting their knowledge to me and for being more than teachers, they have been friends, I will always carry them present in my heart. I also want to thank in a special way Evelyn Cifuentes, who has helped me with great patience and charisma in every question, problem and procedure related to the school.

Thanks to all my family for their support and encouragement during all these years of education, but above all thanks to my mother for always being by my side with her unconditional support in all possible ways and guiding me in my training, thanks to her I am a strong and determined woman. My life will not be enough to thank her for all her unconditional love. To my son for his kisses and hugs when I have needed them most. I also want to say thank you to Anthony, for supporting me over the past few months and believing in me when I wasn't doing it myself.

I thank in a special way: Daya, Mabe, Liss, Stefy, Araceli and Ángel, for being my second family since my first days at university and still by my side, thank you for being with me in the worst and best moments, I will miss a lot the laughter, the walks, but above all sharing my memories with you.

In the same way, I want to thank my school friends who have supported me and helped me with my doubts about my career: Pato, Majo, Tefo, Pancho P, Ronny. The shared laughter made my journey easier. Thank you very much to Jessy, Faby and Andrés, for those nights of laughter and jokes while we did the thesis, even if it was from a distance.

Finally, I thank all the friends I made in university and they have been an essential part in these years: Mayra, Gaby, Juli, Álex, Pancho B, Diego, Juan, Jaylenne, Danny and all those who have been part of some stage of my life university, all have been an emotional support and have left their mark on my heart.

This achievement would not have been possible without the support and presence of all of you in my life, thank you all very much.

Iskra Nicole Zambrano García

## Resumen

La espintrónica molecular en sistemas biológicos ha sido un campo de investigación de gran interés en los últimos años. El descubrimiento experimental del efecto Chiral Induced Spin Selectivity (CISS) en aminoácidos, oligopéptidos y ADN ha llevado a una carrera para explicar este fenómeno desde el punto de vista teórico. El enfoque principal es determinar la fuente de la actividad de espín en soportes orgánicos sin centros magnéticos o átomos pesados y explicar el efecto de polarización de espín muy grande que puede ser mayor que el de las interfaces ferromagnéticas.

En este proyecto, derivamos un modelo analítico de moléculas quirales para explicar el proceso de túnel de electrones como mecanismo de transporte en sistemas biológicos quirales, como el ADN. Se realiza un estudio basado en un modelo analítico de Tight-Binding de una molécula de ADN de doble hélice, con un tipo de par de nucleótidos y un orbital  $\pi$  orientado a bases, en el que se incorporan contribuciones cinéticas e intrínsecas Spin-Orbita (ISO). Como parte de este modelo, se deriva un hamiltoniano consistente con el transporte de carga en este sistema y se detalla el proceso de tunelización que está fuertemente acoplado con la interacción ISO. La actividad de espín se evidenciará mediante un acoplamiento de espín efectivo de primer orden en el hamiltoniano resultante evaluado en la energía de Fermi, a través de cálculos de transporte tales como corrientes de carga, corrientes de espín y densidad de par. Adicionalmente, se desarrolla una técnica para describir sistemas de oligoacenos mediante un hamiltoniano eficaz, mediante el método de diezrado, para ser utilizado como medio para estudiar el transporte cuántico de electrones en estas moléculas.

### **Palabras Clave:**

Espintrónica, quiral, espín, polarización, molécula, transporte, ADN, acoplamiento de espín, tunelización, Fermi, energía, efecto CISS.

## Abstract

Molecular spintronics in biological systems has been a field of research of high interest in recent years. The experimental discovery of the Chiral Induced Spin Selectivity (CISS) effect in amino-acids, oligo-peptides and DNA has led to a race to explain this phenomenon from the theoretical point of view. The main focus is determining the source of the spin activity in organic supports with no magnetic centers or heavy atoms and explain the very large spin polarization effect that can be larger than that of ferromagnetic interfaces.

In this project, we derive an analytical model of chiral molecules to explain the process of electron tunneling as a transport mechanism in biological chiral systems, such as DNA. A study is carried out based on an analytical Tight-Binding model of a double helix DNA molecule, with one type of nucleotide pair and a base-oriented  $\pi$  orbital, in which kinetic and Intrinsic Spin-Orbit (ISO) contributions are incorporated. As part of this model, a Hamiltonian consistent with the charge transport in this system is derived and the tunneling process that is strongly coupled with the ISO interaction is detailed. Spin activity will be evidenced by first order effective spin-coupling in the resulting Hamiltonian evaluated at the Fermi energy, through transport computations such as charge currents, spin currents and torque density. Additionally, a technique is developed to describe Oligoacenes systems by means of an effective Hamiltonian, through the decimation method, to be used as a means of studying quantum transport of electrons in these molecules.

### Keywords:

spintronics, chiral, spin, polarization, molecule, transport, DNA, spin-coupling, tunneling, Fermi, energy, CISS effect.

# Contents

<b>List of Figures</b>	<b>x</b>
<b>List of Tables</b>	<b>xiii</b>
<b>List of Papers</b>	<b>xv</b>
<b>1 Introduction</b>	<b>1</b>
1.1 Problem Statement . . . . .	6
1.2 General and Specific Objectives . . . . .	7
1.2.1 General Objective . . . . .	7
1.2.2 Specific Objectives . . . . .	7
<b>2 Methodology</b>	<b>9</b>
2.1 Overlaps and Slater-Koster Parameters . . . . .	9
2.2 Kinetic Energy Term . . . . .	9
2.3 Intrinsic Spin-Orbit coupling . . . . .	10
2.4 Tight-Binding Hamiltonian For a DNA Model . . . . .	11
2.5 Tunneling through a Potential Barrier . . . . .	15
2.6 Spin Polarization . . . . .	18
2.7 Electron Transport Computations . . . . .	19
2.7.1 Spin Torque Density . . . . .	21
2.8 The Decimation Method . . . . .	22
<b>3 Results &amp; Discussion</b>	<b>25</b>
3.1 Spin-Orbit Interaction and Spin Selectivity for Tunneling Electron Transfer in DNA . . . . .	25
3.1.1 Tight-Binding Hamiltonian . . . . .	25
3.1.2 Potential Barrier . . . . .	27
3.2 Spin Polarization . . . . .	34
3.3 Charge Current. . . . .	36

3.3.1	Region I . . . . .	36
3.3.2	Region II . . . . .	37
3.3.3	Region III . . . . .	39
3.4	Spin Current . . . . .	39
3.4.1	Above barrier energies $E > V_0$ . . . . .	40
3.4.2	Energies below the barrier $E < V_0$ . . . . .	41
3.5	Torque Density . . . . .	41
3.5.1	Above energies barrier $E > V_0$ . . . . .	42
3.5.2	Energies below the barrier $E < V_0$ . . . . .	42
3.6	S wave Hamiltonian for Oligoacenes: Decimation approach . . . . .	43
<b>4</b>	<b>Conclusions &amp; Outlook</b>	<b>51</b>
	<b>Bibliography</b>	<b>53</b>
	<b>Abbreviations</b>	<b>59</b>

# List of Figures

1.1	Physicists who started with the idea of the consideration of the electron spin. a) H.B.G. Casimir, and R. Levensbericht. Ralph Kronig. 1996. Retrieved from <sup>1</sup> . b) P. Halpern. George Uhlenbeck (L) and Samuel Goudsmit (R) came up with the idea of quantum spin in the mid-1920s. This photo was taken with Hendrik Kramers (center) in 1928 (Public Domain). 2017. Retrieved from <sup>2</sup> . . . . .	2
1.2	Spin up and spin down. . . . .	2
1.3	E. E. Fullerton, and I. K. Schuller. Examples of the exciting science and technological advance in magnetic nanoscience. (A) Schematic representation of interlayer coupling between two ferromagnetic layers across a non-magnetic (yellow) spacer layer. As the spacer layer thickness changes, the coupling oscillates between ferromagnetic and antiferromagnetic coupling, resulting in parallel and antiparallel alignment of the magnetization. (B) GMR response from an Fe/Cr superlattice. In zero magnetic field the layers are antiparallel (as indicated by the arrows). Applying a large magnetic field saturates the Fe layers and causes a “giant” decrease in the resistance. (C) Schematic of a spin-transfer device where current can switch the direction of the magnetization of a layer. (D) Schematics of a spin-valve GMR sensor where the reference (blue) magnetic layer is pinned by an antiferromagnetic layer (green) and the free magnetic (red) is separated from the reference layer by a thin conducting spacer (yellow). (E) A hard disk drive which uses a GMR sensor to read the data stored on the disk. (F) Top view of a micro-fluidic magneto-nanochip with an 8x8 GMR sensor array and eight microfluidic channels. (G) Cross-sectional transmission electron microscope image of a 4-megabit toggle MRAM showing backend integration of magnetic tunnel junctions and Cu write lines. 2007. Retrieved from <sup>3</sup> . . . . .	3
1.4	A scheme describing the monolayer of dsDNA as spin filter. Unpolarized electrons are injected from the gold substrate, it is observed that most of the electrons transmitted through DNA are polarized so that their spin is aligned in an antiparallel speed. 2011. Retrieved from <sup>4</sup> . . . . .	5
1.5	A nanoparticle-dsDNA-nickel complex is shown. DsDNA is bound at one extreme to Ni while at the other extreme it is chemically bound to gold nanoparticles. The current is measured between the nickel substrate and an AFM tip. (2011). Retrieved from <sup>5</sup> . . . . .	6
2.1	Scheme of the Slater-Koster parameters, which represent the different types of $\sigma$ and $\pi$ bonds considered in this model. . . . .	10

2.2	Representation of the $p_z$ - $p_z$ overlap between near neighbors, which is described with the kinetic term.	10
2.3	Representation of $p_z - p_z$ coupling between first neighbors through first order ISO interaction and $E_{ys}$ overlap. . . . .	11
2.4	DNA structure. Retrieved and adapted from <sup>6</sup> . . . . .	12
2.5	S. Varela et al. Representation of a base pair in the X-Y plane, where $\phi$ is the angle between consecutive bases and $\varphi$ is a reference angle to the X axis. 2016. Retrieved from <sup>7</sup> . . . . .	13
2.6	S. Varela et al. Structure of the orbitals in the molecule in the XY plane. The $p_x$ orbitals are represented in blue, the $p_y$ orbitals in red and the $p_z$ orbitals in green. The orientation of the $p_z$ orbitals is parallel to the axis of the helix. 2016. Retrieved from <sup>7</sup> . . . . .	14
2.7	S. Varela et al. Each base in the $i$ site has three first neighbors, of which two are on the same DNA strand, $j = 1$ and $j = 2$ , and the third is opposite on the other strand, $j = 3$ . 2016. Retrieved from <sup>7</sup> . . . . .	15
2.8	Scheme of quantum tunneling effect through a potential barrier. . . . .	16
2.9	S. J. Ling et al. Tunneling-quantum problem. In regions I and III the particle moves freely with an oscillatory behavior, while in region II, where the potential barrier is found, the particle has a decay-exponential behavior. 2018. Retrieved and adapted from <sup>8</sup> . . . . .	18
2.10	The charge current consists of the flow of electrons through the potential barrier. . . . .	19
2.11	Scheme of the Spin Current. Electrons with different spin states flow from left to right through the potential barrier. . . . .	20
2.12	Scheme of the Spin Torque. The electrons injected with a spin state, upon entering the potential barrier, undergo a torque force, changing their state. . . . .	22
2.13	H. M. Patawski, and E. Medina. <i>Scheme of the decimation of a finite tight-binding strip. As the elimination of intermediate layers proceeds the effective site energies and interaction appears.</i> 2001. Retrieved from <sup>9</sup> . . . . .	24
3.1	Energy spectrum in the first zone of Brillouin. The points $K_v$ at which the expansion was performed are shown. Retrieved and adapted from <sup>7</sup> . . . . .	26
3.2	Scattering potential barrier model with SO interaction, where $E$ is the energy of the incident electron and $V_0$ is the barrier potential. The labels corresponding to the amplitudes of the wave functions of incidence ( $A$ ), reflected ( $B$ ) and transmitted ( $F$ ) are shown. The ISO interaction is just active on the barrier. . . . .	28
3.3	Spin components probability with energy values near to the barrier potential. A favorable behavior towards a spin component is observed within the barrier, causing a spin polarization. . . . .	34
3.4	Spin asymmetry $P_z$ as a function of $a$ in nm and the velocity of the Spin-Orbit (SO) interaction in m/s. The values for the incident wave function $k = 7 \text{ nm}^{-1}$ and the barrier height $q_0 = 7.24 \text{ nm}^{-1}$ are fixed. . . . .	35
3.5	Spin asymmetry $P_z$ as a function of $a$ in nm and the velocity of the SO interaction in m/s. The values for the incident wave function $k = 5 \text{ nm}^{-1}$ and the barrier height $q_0 = 7.24 \text{ nm}^{-1}$ are fixed. . . . .	36

3.6	Spin asymmetry $P_z$ as a function of $a$ in nm and the velocity of the SO interaction in m/s with the barrier height $q_0 = 7.24 \text{ nm}^{-1}$ . a) The values for the incident wave function $k = 2 \text{ nm}^{-1}$ . b)The values for the incident wave function $k = 1 \text{ nm}^{-1}$ . . . . .	37
3.7	Torque Density $\tau$ in the region II for spin up and down in N.m as a function of the SO interaction in m/s with the incident wave function $k = 7 \text{ nm}^{-1}$ and the barrier height $q_0 = 7.24 \text{ nm}^{-1}$ . . . . .	43
3.8	Torque Density $\tau$ in the region II for spin up and down in N.m as a function of the SO interaction in m/s with the incident wave function $k = 5.12 \text{ nm}^{-1}$ and the barrier height $q_0 = 7.24 \text{ nm}^{-1}$ . . . . .	44
3.9	Torque Density $\tau$ in the region II for spin up and down in N.m as a function of the SO interaction in m/s with the incident wave function $k = 1 \text{ nm}^{-1}$ and the barrier height $q_0 = 7.24 \text{ nm}^{-1}$ . . . . .	45
3.10	Scheme of the decimation method applied to a Benzene molecule. . . . .	45
3.11	Scheme of the decimation method in Oligoacenes. a)Naphthalene, b)Anthracene, c)Tetracene, d)Pentacene, e)Hexacene . . . . .	46
3.12	Full Hamiltonian of Oligoacenes. a) Naphtalene, b) Anthracene and c) Tetracene . . . . .	47



# List of Tables

3.1	Inflection points $K_v$ used to apply a small perturbation . . . . .	26
3.2	Parameters of the spin components probability $\psi^2$ . . . . .	33



# List of Papers

- [1] Spin-orbit interaction and spin selectivity for tunneling electron transfer in DNA, PHYSICAL REVIEW B 101, 241410(R) (2020).



# Chapter 1

## Introduction

The technological devices which have been developed throughout history have been based on the *charge* of electrons that can be acted on by external electric and magnetic fields. However, since the end of the last century, devices focused on nanoscale electronic circuits with the object of detection and manipulation of an intrinsic property that electrons possess<sup>10</sup>, namely *spin*. The manipulation of the spin degree of freedom and the control over the electric charge is a field of research in the area of physics, called *spintronics*. This spin-based electronics is one of the most important emerging areas of nanotechnology including highly active areas in nanomagnetism, magnetoresistivity, spin injection, optical orientation, spin polarized transport, spin filters, spin valves among many others<sup>11</sup>. This area has already seen the transition from fundamental physics to technological applications in a record time of ten years and is very promising for the future.<sup>12</sup>

Spintronics made its debut in the 80s of the last century, however, spin was discovered many years before. In 1920 many researchers realized that to fully describe the behavior of electrons a fourth concept was missing in addition to the "classical" quantum numbers<sup>13</sup>. The additional number was speculated to be due to the fact that electrons could rotate about their own axis. The first experimental evidence of the existence of the spin came in the year 1922 in an experiment carried out by Otto Stern and Walther Gerlach<sup>14</sup>. In this experiment they reported, by means of a silver atom, that there was a magnetic moment present. In 1925 three physicists: Ralph Kronig, Samuel Goudsmit and George Uhlenbeck (see Fig.1.1) started from the idea that the electron rotates on its own axis, similar to the Earth, and they realized that adding a quantum number associated to this *spin*, it was possible to give a complete explanation of most atomic spectra<sup>15</sup>.

Thanks to the previous conclusions, a definition for spin could be given. The spin is an intrinsic property of the electron, that accounts for an intrinsic magnetic moment. For spin 1/2 particle, the particle has two possible states; "spin up" and "spin down" (see Fig.1.2) with respect to a predetermined quantization axis. A current of electrons, carrying spinfull carriers in the two states, carries information and interacts in a characteristic fashion with magnetic materials<sup>16</sup> through e.g. magnetic dipole or Zeeman couplings. For these reasons, spintronics has generated a great impact through the development of spin-based systems, such as hardware for storing information and sensors or magnetic data, magneto-mechanical oscillators, among other applications<sup>17</sup>.

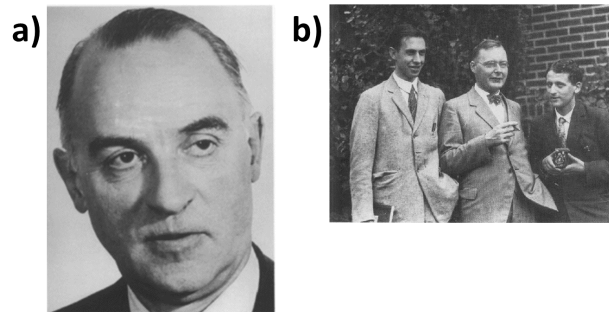


Figure 1.1: Physicists who started with the idea of the consideration of the electron spin. a) H.B.G. Casimir, and R. Levensbericht. Ralph Kronig. 1996. Retrieved from<sup>1</sup>. b) P. Halpern. George Uhlenbeck (L) and Samuel Goudsmit (R) came up with the idea of quantum spin in the mid-1920s. This photo was taken with Hendrik Kramers (center) in 1928 (Public Domain). 2017. Retrieved from<sup>2</sup>.

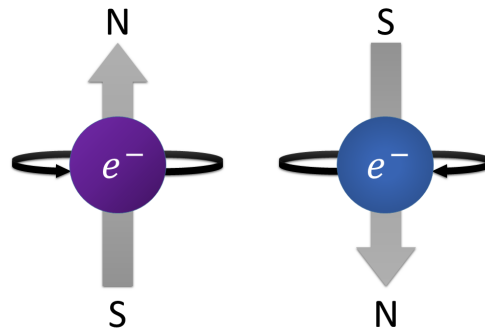


Figure 1.2: Spin up and spin down.

One of the first successes in spintronics, using the electron spin to process information, was the discovery of the Giant Magneto-Resistance (GMR) in magnetic multilayers with nanometric thicknesses by researchers Albert Fert and Peter Grünberg<sup>18,19</sup>, which showed that the electrical resistance of a magnetic device can be modified by changing its magnetic texture. This phenomenon was named Giant Magneto-resistance or GMR. Therefore, this effect could be used for different electronic devices as shown in the Fig. 1.3. This incredible scientific discovery spread rapidly in the industry, just a few years later IBM launched the first commercial device based on this effect (1988), which was a computer hard disk that used the GMR as the reading mechanism of the information. As a consequence of this work, these researchers were awarded the Nobel Prize in Physics in 2007<sup>3</sup>. Another notable although not realized proposal is the Datta-Das transistor that uses spin precession, in the presence of the Spin-Orbit

coupling (SOC), to realize switching<sup>20</sup>.

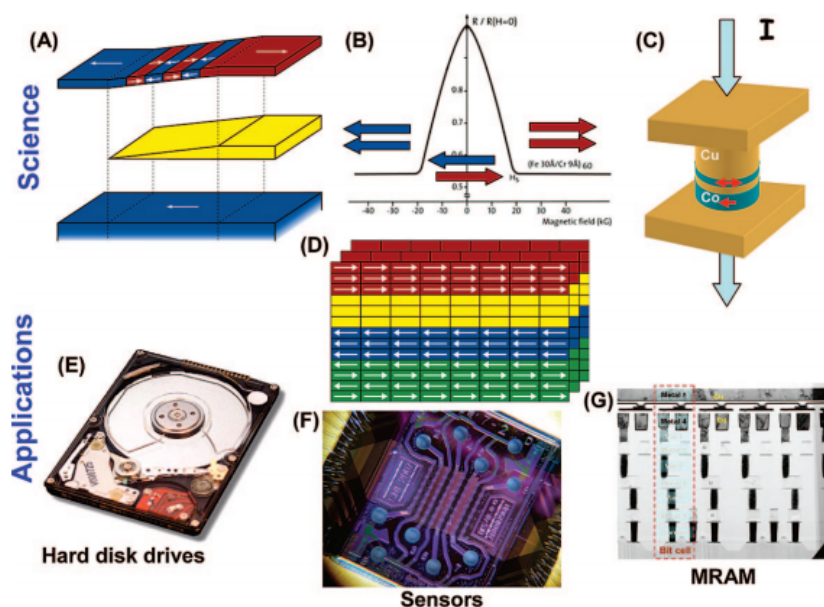


Figure 1.3: E. E. Fullerton, and I. K. Schuller. Examples of the exciting science and technological advance in magnetic nanoscience. (A) Schematic representation of interlayer coupling between two ferromagnetic layers across a non-magnetic (yellow) spacer layer. As the spacer layer thickness changes, the coupling oscillates between ferromagnetic and antiferromagnetic coupling, resulting in parallel and antiparallel alignment of the magnetization. (B) GMR response from an Fe/Cr superlattice. In zero magnetic field the layers are antiparallel (as indicated by the arrows). Applying a large magnetic field saturates the Fe layers and causes a “giant” decrease in the resistance. (C) Schematic of a spin-transfer device where current can switch the direction of the magnetization of a layer. (D) Schematics of a spin-valve GMR sensor where the reference (blue) magnetic layer is pinned by an antiferromagnetic layer (green) and the free magnetic (red) is separated from the reference layer by a thin conducting spacer (yellow). (E) A hard disk drive which uses a GMR sensor to read the data stored on the disk. (F) Top view of a micro-fluidic magneto-nanochip with an 8x8 GMR sensor array and eight microfluidic channels. (G) Cross-sectional transmission electron microscope image of a 4-megabit toggle MRAM showing backend integration of magnetic tunnel junctions and Cu write lines. 2007. Retrieved from<sup>3</sup>.

Historically, spintronics has been used in many inorganic materials since once the magnetic orientation of the material is known, many properties can be improved for later technological use<sup>12,21,22</sup>. Nevertheless, recently, researchers have focused on less conventional sets of materials, such as organic materials<sup>17,23</sup>. In recent years, there have been many pioneering experiments and theoretical works which suggest that organic materials may offer a new route to spintronics because they can offer similar or superior performance in spin device manufacturing than

inorganic materials. This is mainly due to the indisputable advantage of weak spin-orbit and hyperfine interactions in organic molecules, which leads to the possibility of preserving spin coherence at times and distances much longer than in conventional metals or semiconductors<sup>24</sup>. Additionally, organic molecules have many types and combinations of preparation, they are synthesized at low temperature, their properties can be finely adjusted and their degree of purity can be higher than in the inorganic world. Even so, what has mostly inspired the study of spintronics in organic molecules is the fact that they possess an extremely wide range of functionality and electronic properties. This new area of research, which has been inspired by pioneering spin transport experiments<sup>25</sup> and the first theoretical predictions<sup>24</sup> through organic molecules, has been called Molecular Spintronics. These investigations include carbon nanotube spin valves<sup>26</sup>, coherent spin transfer of hot electrons across molecular bridges<sup>27</sup>, injection of spin into  $\pi$ -conjugated molecules<sup>23,25</sup>, etc. All these works show the spintronic properties possessed by these molecules and as can be manipulated to the required function.

One of the spintronic phenomena which has emerged in recent years, and shows great promise for new spintronic devices, catalysis, and biological electron transfer is the Chiral Induced Spin Selectivity (CISS) effect, which describes the spin filtering capacity of diamagnetic helical structures such as DNA or peptides that possess chiral symmetry<sup>28-33</sup>. Chiral molecules are those that do not have parity symmetry, that is, they do not overlap in their mirror image, like the left and right hand, so a mirror symmetry operation transforms one enantiomer into another<sup>34,35</sup>.

Several experiments have been carried out with chiral organic molecules which, together with the results of other theoretical works, have established firm bases that the transport of electrons, the transfer of electrons or the polarization of bonds in extended chiral systems translates into spin polarization of electrons<sup>36-38</sup>. Many of these studies have obtained results of strong polarization or spin selectivity with this type of molecules, reaching up to 60% polarization<sup>7</sup>. The first experimental revelations of the existence of the CISS effect were obtained by Naaman et al.<sup>39</sup> through electron photoemission studies in experiments with Langmuir-Blodgett type monolayers<sup>40,41</sup> composed of films of chiral molecules Lysine in left-handed (L) and right-handed (D) configurations, deposited on a gold substrate. They concluded that the spin selectivity they observed is unequivocally linked to the chiral nature of the molecules, since the longitudinal component of preferential spin in transmission changed direction under a change in chirality and the lack of it killed any spin activity due to its low atomic weight. Another important experiment was carried out in 2011 by Göhler and collaborators<sup>4</sup>. In their work, they study the transmission of electrons through self-assembled monolayers of double-stranded DNA molecules (SAMs) oriented vertically on a gold substrate. Their results showed that, by expelling photoelectrons by means of a laser pulse whose photons have enough energy to tear the electrons out of the substrate without ionizing the molecules, regardless of their polarization, the electrons were polarized with their spins aligned antiparallel to their speed (see Fig.1.4). Therefore, DNA molecules act as an excellent spin filter, that is, they have the ability to polarize the spin with a relatively high percentage.

A relevant experiment was carried out by Xie et al, in which they studied the CISS effect in the regime of tunneling energies, by means of conductivity measurements of double-stranded DNA molecules<sup>5</sup>. In this work, DNA molecules were deposited on a nickel substrate in such a way that they chemically attached, while their upper

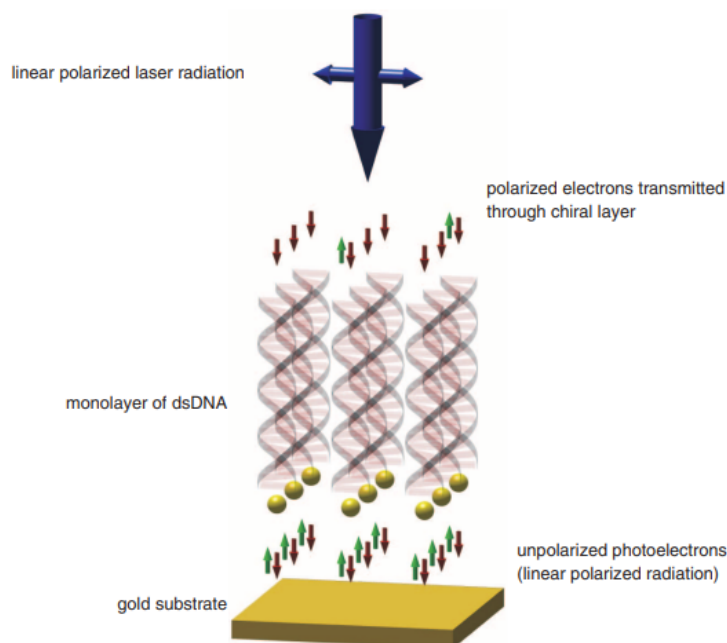


Figure 1.4: A scheme describing the monolayer of dsDNA as spin filter. Unpolarized electrons are injected from the gold substrate, it is observed that most of the electrons transmitted through DNA are polarized so that their spin is aligned in an antiparallel speed. 2011. Retrieved from<sup>4</sup>

ends were chemically joined to a gold nanoparticle, forming a Ni-DNA-Au type system as shown in the figure 1.5. In addition, a magnet was placed under the substrate to monitor the magnetism and therefore the spin alignment in the nickel. Furthermore, a conductive AFM was used to measure the current that flows between the substrate through the DNA to the gold nanoparticle. In their results they obtained that there is a dependence of the conductance of the molecule with the direction of the applied magnetic field and with the length of the molecule, for which they conclude their results are consistent with a DNA spin selectivity.

Theoretically, several investigations show that this effect is attributed to Intrinsic Spin-Orbit (ISO) coupling, which is interesting since there are no heavy elements in these molecules, they only have light atoms such as Carbon, Hydrogen, Oxygen and Nitrogen. However, there is a wide range of analytical theoretical analyzes which link the CISS with the ISO<sup>7,31–33,36,38,42,43</sup>. The first atomistic approaches to describe CISS theoretically used tight binding models with effective ad-hoc parameters which define the Hamiltonian, however, they could not explain the incredible magnitude of the CISS effect, only underestimating it by several orders of magnitude<sup>28</sup>. Therefore, it has been important to investigate the electronic structure of these molecules to obtain what is needed in the theoretical approaches to explain this effect.

There are several studies which show electronic transfer in biological systems is fast and efficient, and it can

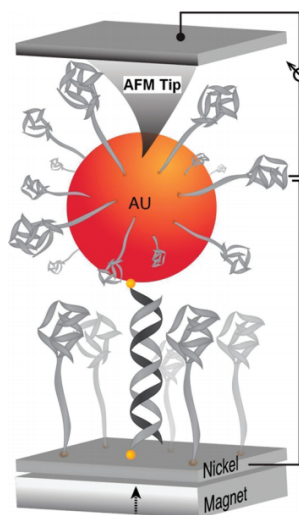


Figure 1.5: A nanoparticle-dsDNA-nickel complex is shown. DsDNA is bound at one extreme to Ni while at the other extreme it is chemically bound to gold nanoparticles. The current is measured between the nickel substrate and an AFM tip. (2011). Retrieved from<sup>5</sup>.

be explained through tunneling processes through organic molecules<sup>38,44–46</sup>. One of the first to develop a theory in terms of tunneling through a potential barrier to analyze electron transfer in biological systems was Hopfield<sup>47,48</sup>, which provided a mechanism to understand the function of structural characteristics of cells. Electron transport molecules and found the expected exponential decrease with spatial separation of localized states. From this, it has been shown this transfer by quantum tunneling occurs at distances between 20 – 40 Å, in biological molecules such as proteins and DNA<sup>49,50</sup>, due to the long-distance transfer of electrons in Proteins and DNA decrease with distance, reinforcing the electron tunneling process as a transport mechanism in these systems. In 2016, Varela et al. derived a Hamiltonian to describe a DNA molecule, taking into account its geometric structure and different atomic interactions, such as the ISO, Stark and Rashba interactions<sup>7</sup>. For our model we start from this Hamiltonian but taking into account only the contribution of kinetic energy and the ISO interaction.

## 1.1 Problem Statement

Molecular spintronics has had high relevance in recent years and has been a field of research considered fascinating due to the properties observed in these biological systems. One of the effects that has shown great promise for electronic devices, catalysis, and biological electron transfer has been the CISS effect on chiral molecules such as amino-acids, oligopeptides, and DNA. Understanding this effect could mean great progress toward new electronic devices with greater efficiency and smaller size. Therefore, its experimental discovery has led much of the scientific

community to search theoretical explanations for this quantum phenomenon. However, it has not been possible to fully explain how these molecules come to possess such magnitude of spin polarization despite the different theoretical models that have been proposed about these molecular systems. A theoretical approach which can explain this quantum effect is the tunneling process through these organic molecules, which can be linked to an ISO coupling. However, the active spin tunneling effect in chiral molecules has not received considerable attention despite its relevance to transport in molecules. This was our motivation to derive an analytical model that explains the CISS effect in chiral biological systems, based on the tunneling process with a strong coupling to the ISO interaction as a transport mechanism for these molecular systems.

## 1.2 General and Specific Objectives

### 1.2.1 General Objective

The general objective of this thesis work is to develop a theoretical analytical model which explains at a physical level the spin selectivity which exists in chiral molecules, such as DNA. In order to do this, we propose doing it through calculations detailing the tunneling process coupled with the ISO interaction as a transport mechanism in these systems. In this way, we pursue to contribute to the study of the spintronic properties that chiral molecules possess, through this analytical method.

### 1.2.2 Specific Objectives

- Derive a Hamiltonian consistent with the charge transport of a DNA molecule considering the ISO coupling.
- Carry out a study through calculations detailing the tunneling process coupled to the ISO interaction as a transport mechanism in DNA.
- Analyze the spin selectivity for the DNA model used, through some computations.
- Develop a technique to study electron transport in Oligoacenes (Benzene Chains), using the decimation method.



# Chapter 2

## Methodology

This chapter explains the theoretical background used in this work to obtain the subsequent results.

### 2.1 Overlaps and Slater-Koster Parameters

The wavefunction overlaps and couplings between  $p_z$  orbitals considered in this model are derived from a Slater-Koster TB analytical approach. The Slater-Koster terms overlaps represent the contribution of orbital overlap in molecular structures. The orbital superposition can be represented as a linear function of the wave functions which describe the orbitals in a proper base, then, if the superposition between two atomic orbitals  $\phi_{l,m} = |l, m\rangle$  is considered, represented by their angular momentum  $l = s, p, d...$  and the magnetic quantum number  $m$ , located in the positions  $\mathbf{R}$  and  $\mathbf{R}'$ , the transfer and overlap integrals are:

$$V_{l'l'm|\delta_{mm'}} = \langle l', m', \mathbf{R}' | \hat{H} | l, m, \mathbf{R} \rangle \quad (2.1)$$

These terms are called Slater-Koster parameters if the relative vector  $\mathbf{R} - \mathbf{R}'$  is parallel to the quantization axis of the  $\phi_{lm}(\mathbf{r} - \mathbf{R}) = \langle \mathbf{r} | l, m, \mathbf{R} \rangle$  orbitals<sup>51,52</sup>. Each value of  $m$  is associated with the different types of bonds between the orbitals by the superposition of their atomic wave functions. Therefore, the magnetic numbers  $m = 0, 1, 2$  represent bonds of type  $\sigma, \pi, \delta$ , respectively, as denoted in figure 2.1. The number of parameters is given by the number of possible combinations of two orbitals and by the type of bond formed. In the model used in this work, only the  $s$  and  $p$  orbitals are considered, so we have the parameters  $V_{ss}^\sigma, V_{sp}^\sigma, V_{pp}^\sigma, V_{pp}^\pi$ .

### 2.2 Kinetic Energy Term

The kinetic term represents one of the couplings between the  $p_z$  orbitals in different bases of the molecule, this term is entirely due to the  $E_{zz}$  overlap of the eigenfunctions between the  $p_z - p_z$  orbitals of near neighbors and preserves the

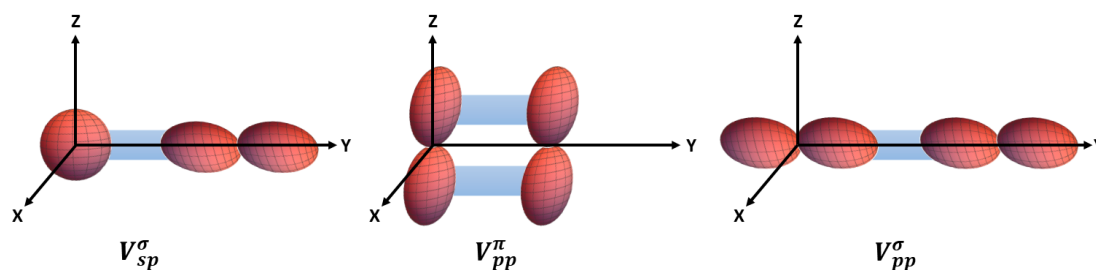


Figure 2.1: Scheme of the Slater-Koster parameters, which represent the different types of  $\sigma$  and  $\pi$  bonds considered in this model.

orientation of the spin (see Fig.2.2). This process occurs both intra-helix (A-A / B-B), and inter-helix (A – B/B – A). The Hamiltonian that describes the DNA molecule includes this kinetic term  $t$ .

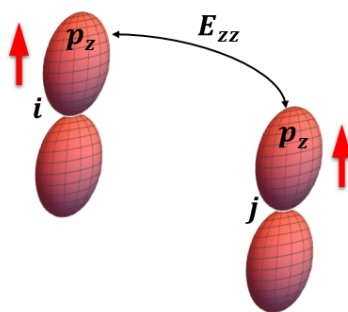


Figure 2.2: Representation of the  $p_z$ - $p_z$  overlap between near neighbors, which is described with the kinetic term.

## 2.3 Intrinsic Spin-Orbit coupling

Intrinsic Spin-Orbit (ISO) coupling is a relativistic coupling between the angular momentum of a particle moving at a potential and the spin of the particle. This relativistic effect starts from the assumption that the nucleus surrounds the electron where the spin magnetic moment and the orbital angular momentum interact, and this creates a magnetic field<sup>53</sup>. This coupling is responsible for the electron spin degrees of freedom being affected by its orbital state and allows a new path between the  $\pi$  orbitals of bases which are near neighbors. The moving electrons from the  $p_z$  orbital are transferred to the  $p_{x,y}$  orbitals of the same base, which causes the spin to flip, and then are transferred through orbital overlap to the  $p_z$  orbitals of the near neighbors. The figure 2.3 represents this coupling process considering the  $p_y$  orbital.

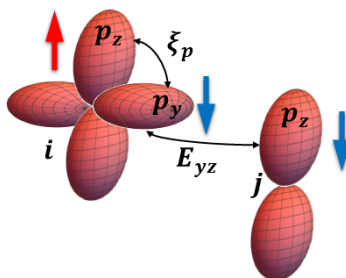


Figure 2.3: Representation of  $p_z - p_z$  coupling between first neighbors through first order ISO interaction and  $E_{yz}$  overlap.

## 2.4 Tight-Binding Hamiltonian For a DNA Model

DNA is a molecule which appertains within the category of polymers. This consists of two chains which wind between them to form a double helix structure. Each chain has a central part made up of sugars (deoxyribose) and phosphate groups. Attached to each sugar is one of the 4 nitrogenous bases that DNA has: Adenine (A), Cytosine (C), Guanine (G) and Thymine (T); and the order in which they combine one after the other is what encodes the genetic information. The two chains remain coupled or linked by hydrogen bonds between these nitrogenous bases<sup>54</sup>. The length of these hydrogen bonds is around 3 Å. Nitrogen bases in DNA are planar organic molecules linked by  $sp^2$ -type hybridization, such as graphene. In the most common configuration of DNA, B-DNA, these bases are oriented in such a way that the plane of the molecules is almost perpendicular to the axis of the double helix, with an angle of inclination of  $1,2^\circ$ . For this reason, the  $p_z$  orbitals of its atoms are perpendicular to the molecular plane. Due to their hybridization and the atoms that make up the base, the electrons which occupy these atomic orbitals are unpaired to form  $\pi$ -type molecular orbitals. In the aforementioned configuration, the DNA structure presents a dextro-rotatory chirality, that is, it has a clockwise rotation seen from the bottom up and the pitch has a length of 35.4Å (see Fig.2.4) with 10.4 base pairs per turn, besides the angle between two consecutive base pairs is  $34.6^\circ$ .

The DNA structure model used in this work is the one developed by Varela et al.<sup>7</sup>. The phosphate groups of the molecule do not contribute in this model because all the conduction of electrons occurs in the internal structure where the bases are, since the conducting electrons are contributed by the nitrogenous bases due to their type of hybridization. In addition to this, the bases are well located so they can be modeled as a set of orbitals per site. Therefore, a double helix structure is considered where each nitrogenous base is represented by a  $p_z$ -type orbital oriented perpendicular to it and s and p orbitals in the plane representing the outer shell of a carbon atom. Each atom that represents a DNA base has an unpaired electron in the  $p_z$  orbital, which is the moving electron<sup>55</sup>. The bases connecting the two helices are separated by a distance equal to the diameter of the structure.

Position vectors for a nitrogenous base pair can be represented as shown in Fig.2.5. A base pair is represented at site  $i$  with the labels  $\mathbf{R}_i$  and  $\mathbf{R}'_i$ , where the first term indicates the base of one helix and the second the base of the

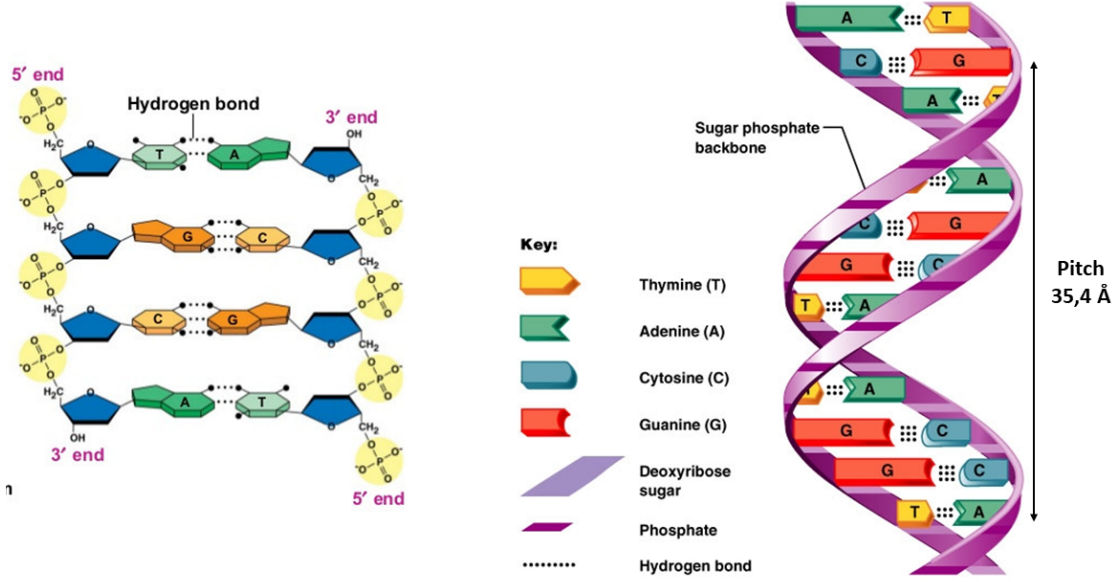


Figure 2.4: DNA structure. Retrieved and adapted from<sup>6</sup>.

other helix. This vector can be described as:

$$\mathbf{R}_i = a \cos[\varphi + (i-1)\Delta\phi] \hat{X} + a \sin[\varphi + (i-1)\Delta\phi] \hat{Y} + \frac{(i-1)\Delta\phi}{2\pi} b \hat{Z}, \quad (2.2)$$

where  $b$  is the pitch of the helix,  $a$  the radius of the helix,  $\Delta\phi$  the angle between two consecutive bases of the same helix and  $\varphi$  is the reference angle with respect to the  $\hat{X}$  axis of the fixed coordinate system.

Other geometric relationships of the DNA structure are deduced taking into account the number of nitrogenous bases and the number of turns of the molecule. For this system,

$$\mathcal{N} = \frac{N-1}{M-1}, \quad (2.3)$$

and

$$\Delta\phi = \frac{2\pi}{(M-1)}, \quad (2.4)$$

are satisfied, where  $N$  is the number of base pairs considered in the structure,  $\mathcal{N}$  is the number of turns of the helices and  $M$  is the base pairs that each turn contains.

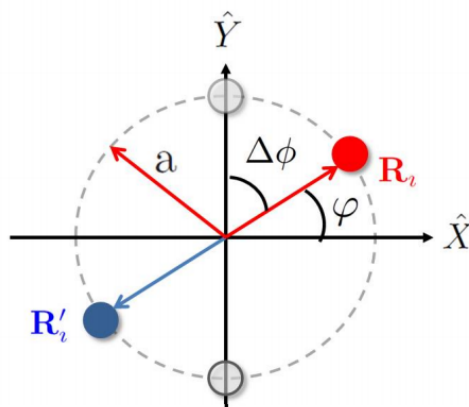


Figure 2.5: S. Varela et al. Representation of a base pair in the X-Y plane, where  $\phi$  is the angle between consecutive bases and  $\varphi$  is a reference angle to the X axis. 2016. Retrieved from<sup>7</sup>.

For the Hamiltonian construction, the two bases in opposite positions of the same pair are distinguished by the labels  $A$  and  $B$ , sub-understanding a pseudo-spin space. There is an orientation of the orbitals in each base with a given local system as shown in the figure 2.6. The  $p_x$  and  $p_y$  orbitals are distributed in the  $X - Y$  plane of the fixed system with a ring-shaped approximation, but due to the structure of the helix, they have an additional component in the direction of the  $Z$  axis, which is directly related to the chirality of the molecule. For this DNA model, a tight binding model is used, so only strong or important interactions are considered, that is, those which are first neighbors. As described in Fig.2.7, each site  $i$  has 3 first neighbors  $j$ , two on the same helix and one on the opposite helix. The distance between these neighboring atoms becomes:

$$|\mathbf{R}_{ji}|^2 = \frac{16\pi^2 a^2 \sin^2\left(\frac{\Delta\phi}{2}\right) + (b\Delta\phi)^2}{4\pi^2}. \quad (2.5)$$

This equation is consistent, since when it is about two atoms with different helices ( $\Delta\phi = \pi$  and  $b = 0$ ) their distance is equal to  $2a$ , corresponding to the diameter of the helix.

The overlapping neighboring orbitals which occur in this structure have both  $\pi$  and  $\sigma$  components. However, due to the helical/chiral structure that this molecule possesses, additional overlaps occur between the  $p_z$  orbitals due to intra-atomic orbital coupling interactions. One of them that occurs in this system and is considered in this work is a first order Spin-Orbit (SO) coupling, similar to that of carbon nanotubes<sup>56</sup>. Wavefunction overlays and SO couplings are derived from a Tight-Binding Slater-Koster analytical approach with lowest order perturbation theory. Varela et al.<sup>7</sup> derived, from these considerations, a complete Hamiltonian, however, in this work we consider the major contributions to the Hamiltonian, but only with the ISO coupling of the atoms involved in the  $\pi$  orbitals (N, C, O). Consequently, the Hamiltonian used is comprised of two terms, as described by:

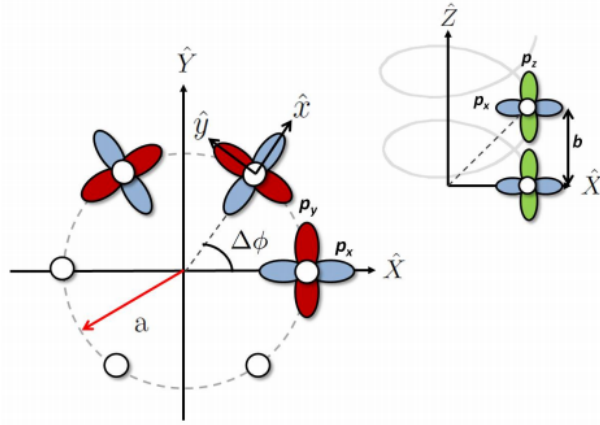


Figure 2.6: S. Varela et al. Structure of the orbitals in the molecule in the  $XY$  plane. The  $p_x$  orbitals are represented in blue, the  $p_y$  orbitals in red and the  $p_z$  orbitals in green. The orientation of the  $p_z$  orbitals is parallel to the axis of the helix. 2016. Retrieved from<sup>7</sup>.

$$H = (\varepsilon_{2p}^\pi + 2t f(k)) \mathbf{1}_s - 2g(k) \lambda_{SO} \mathbf{s}_y, \quad (2.6)$$

where  $\mathbf{1}_s$  represents the unit matrix in spin space and  $\mathbf{s}_y$  is the Pauli matrix representing the spin degree of freedom in the local coordinate system of the molecule.

As mentioned above, the Hamiltonian has two terms, the first implies the term  $\varepsilon_{2p}^\pi$  which corresponds to the base  $2p\pi$  orbital energy and the kinetic energy  $t$ , which is defined as:

$$t = V_{pp}^\pi + \frac{b^2 \Delta\phi^2 (V_{pp}^\sigma - V_{pp}^\pi)}{8\pi^2 a^2 (1 - \cos\Delta\phi) + b^2 \Delta\phi^2}. \quad (2.7)$$

The above expression shows this overlap depends on the angle  $\Delta\phi$  between the bases and the  $b$  parameter of the helix, and involves both  $\pi$  and  $\sigma$  components. When  $b = 0$ , that is, when the overlap is between two bases of the two helices (between sublattices  $A$  and  $B$ ), the kinetic term is reduced to the Slater-Koster parameter corresponding to the  $\pi$  bond between the  $p_z$  orbitals of the bases.

The second term,  $\lambda_{SO}$ , corresponds to the effective molecular ISO coupling or the active spin term:

$$\lambda_{SO} = \frac{4\pi\xi_p r b \Delta\phi (1 - \cos\Delta\phi) (V_{pp}^\sigma - V_{pp}^\pi)}{(\varepsilon_{2p}^\pi - \varepsilon_{2p}^\sigma) (8\pi^2 r^2 (1 - \cos\Delta\phi) + b^2 \Delta\phi^2)}, \quad (2.8)$$

where  $\xi_p$  is the coupling of atomic SO of atoms with double bonds in the bases (either C, O or N) and  $\varepsilon_{2p}^{\pi,\sigma}$  are the bare energies if the  $2p$  valence orbital is  $\pi$  (perpendicular to the base) or bound  $\sigma$ . This equation makes notice this coupling is dependent on the chirality of the helix, since if  $b$  is equal to zero, do not have this contribution in the Hamiltonian. Finally, it is important to emphasize the equations of the parameters  $\lambda$  and  $t$  include all the geometric

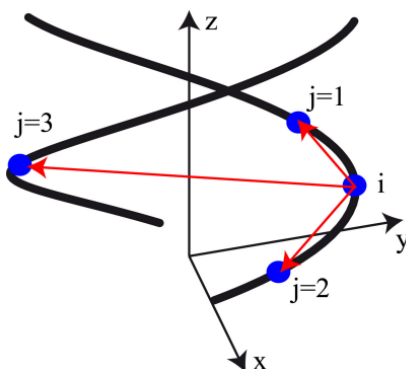


Figure 2.7: S. Varela et al. Each base in the  $i$  site has three first neighbors, of which two are on the same DNA strand,  $j = 1$  and  $j = 2$ , and the third is opposite on the other strand,  $j = 3$ . 2016. Retrieved from<sup>7</sup>.

characteristics of the DNA helix.

Additionally, the functions  $f(k)$  and  $g(k)$  correspond to the functions of the reciprocal space with the lattice parameter  $R$  and the wave vector  $k$  in the local system of the helix, and are shown in equations 2.9 and 2.10. In the Hamiltonian, the terms that have the most relevance are those of kinetic energy and active spin, since they represent the couplings which are considered in this model, which are explained below.

$$f(k) = \cos(\mathbf{k} \cdot \mathbf{R}) \quad (2.9)$$

$$g(k) = \sin(\mathbf{k} \cdot \mathbf{R}) \quad (2.10)$$

## 2.5 Tunneling through a Potential Barrier

Quantum tunneling is one of the most amazing quantum phenomena. The term encompasses a large number of different effects which have in common the possibility that a quantum system is in a classically forbidden region of space, so that, it violates the principles of classical mechanics<sup>57</sup>. One of the researchers who has analytically clarified this phenomenon in recent years is Mohsen Razavy with his book *Quantum Theory of Tunneling*, in which he describes the quantum theory of tunnel construction<sup>58</sup>.

The quantum tunneling phenomenon refers when the particles are able to cross or penetrate a potential energy barrier  $V_0$  with a height greater than the total kinetic energy  $E$  of the particles (see Fig.2.8). This surprising property of certain particles plays an essential role in various physical phenomena, such as alpha decay and nuclear fusion. In addition, it has several important applications, such as the tunnel diode, quantum computing, and the Scanning

Tunneling Microscope (STM), which have had a profound impact on physical, chemical, biological, and materials science research.

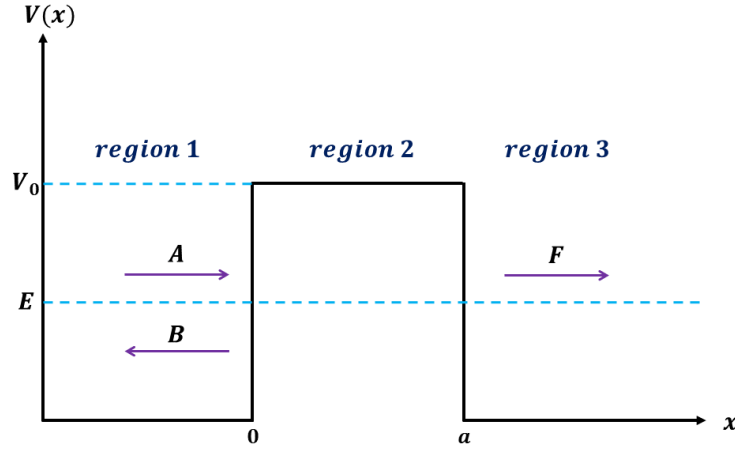


Figure 2.8: Scheme of quantum tunneling effect through a potential barrier.

Tunneling is explained by the Heisenberg uncertainty principle and the wave-particle duality of matter. Microscopic particles such as protons and electrons possess this nature of duality. The uncertainty principle defines a limit on the precision with which the position and momentum of a particle can be known at the same time. In order to describe the behavior of these particles, a complex function is associated, called a wave function. The wave function  $\psi$ , which is a function of the time and the position of all the particles in the system, is a solution of the Schrödinger wave equation, and the probability of finding particles in a certain place is given by  $|\psi|^2$ .

We assume that a uniform, time-independent beam of electrons with energy  $E$  traveling along the  $x$  axis, in the positive direction to the right, encounters a potential barrier described by:

$$V(x) = \begin{cases} 0 & ; \quad x < 0, \\ V_0 & ; \quad 0 \leq x \leq a, \\ 0 & ; \quad x > a. \end{cases} \quad (2.11)$$

In order to find the probability that the beam particles pass through the barrier, we solve the boundary value problem for the time-independent Schrödinger equation. First, we must solve the eigenvalue problem of equation 2.12 for each of the regions. The general form of this equation is given by,

$$H\psi = E\psi, \quad (2.12)$$

$$-\frac{\hbar^2}{2m} \frac{\partial^2 \psi(x)}{\partial x^2} + V(x)\psi(x) = E\psi(x). \quad (2.13)$$

Knowing that the total kinetic energy  $E$  is less than  $V_0$ , as shown in figure 2.8, and taking into consideration that  $V_0$  corresponds to the values shown in Eq.2.11, a solution is sought for the wave functions in each region. The general solutions of the time-independent Schrödinger equation in the three regions are:

$$\begin{aligned} \text{region 1} & : \psi_I = Ae^{ikx} + Be^{-ikx} \quad ; \quad x < 0, \\ \text{region 2} & : \psi_{II} = Ce^{\kappa x} + De^{-\kappa x} \quad ; \quad 0 \leq x \leq a, \\ \text{region 3} & : \psi_{III} = Fe^{ikx} \quad , \quad x > a, \end{aligned} \quad (2.14)$$

where  $k = \frac{\sqrt{2mE}}{\hbar}$  and  $\kappa = \frac{\sqrt{2m(V-E)}}{\hbar}$  are the wave vectors for the electron.  $\psi_I$  corresponds to the left of the barrier, and it can be expressed as a sum of the incident and reflected waves, so  $A$  is the incident amplitude and  $B$  is the reflected amplitude. On the other hand,  $\psi_{III}$  corresponds to the right of the barrier, and it becomes the waves transmitted, so that  $F$  is the transmitted amplitude. The constants  $A, B, C, D, F$  are determined from the wave function  $\psi(x)$  and its derivative  $\partial_x \psi(x)$  with the continuity condition at  $x = 0$  and  $x = a$ . The constants  $A, B$ , and  $F$  can be complex.

The continuity condition of  $\psi(x)$ , at  $x = 0$ , requires:

$$\psi_I(x = 0) = \psi_{II}(x = 0), \quad (2.15)$$

and

$$\partial_x \psi_I(x = 0) = \partial_x \psi_{II}(x = 0), \quad (2.16)$$

whereas the  $\partial_x \psi(x)$  continuity condition, at  $x = a$ , requires:

$$\psi_{II}(x = a) = \psi_{III}(x = a), \quad (2.17)$$

and

$$\partial_x \psi_{II}(x = a) = \partial_x \psi_{III}(x = a). \quad (2.18)$$

By performing these calculations, the path of the electrons for this system can be observed. The electrons start out as a sine wave, then one part of this beam is reflected while the other begins to tunnel through the barrier and goes into exponential decay until it leaves the barrier and is transmitted to the other side as a final sinusoidal wave, but with a smaller amplitude (see Fig.2.9). The act of tunneling decreases the amplitude of the wave due to the reflection of the incident wave when it comes into contact with the barrier, but it does not affect the equation of the wave<sup>59,60</sup>. The amount of incident wave which can pass through a barrier, depends on the width of the barrier, its height  $V_0$  and the energy  $E$  of the incident particles on the barrier.

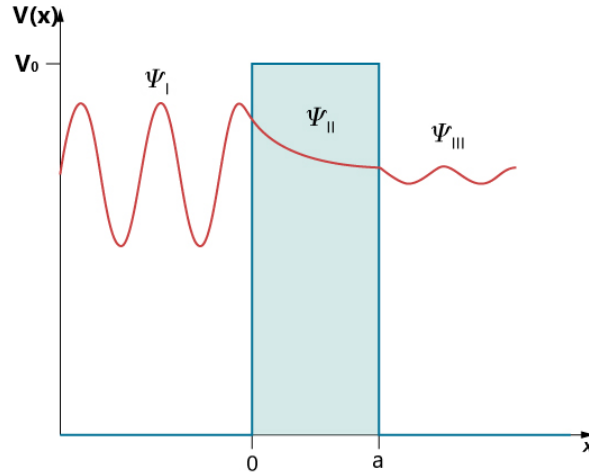


Figure 2.9: S. J. Ling et al. Tunneling-quantum problem. In regions I and III the particle moves freely with an oscillatory behavior, while in region II, where the potential barrier is found, the particle has a decay-exponential behavior. 2018. Retrieved and adapted from<sup>8</sup>

## 2.6 Spin Polarization

Spin polarization in electronic systems is a fundamental phenomenon associated with electron-electron interactions<sup>61</sup>. The study of electron spin polarization deals with sets of electrons in which one of the two possible states is preferentially populated. In materials showing this polarization, the electron bands with up and down spin differ from each other. At the Fermi energy level, the fillings of both bands are different and the densities of states are also different for both types of carriers. Thus, the spin polarization is conceptualized as the normalized difference in the density of states (DOS) of spin carriers up and down at the Fermi level<sup>62</sup>.

As a consequence, this polarization will depend on the relationship between the densities of electrons with spin up and down, and the degree of polarization is given by the fractional difference of populations of the two spin states, as indicated by<sup>62-64</sup>:

$$P_z = \frac{N_\uparrow - N_\downarrow}{N_\uparrow + N_\downarrow}, \quad (2.19)$$

where  $N_\uparrow$  ( $N_\downarrow$ ) are the number of electrons with spins parallel (antiparallel) to a quantization direction.

One of the methods for making a quantitative analysis of the spin polarization in various materials has been tunneling effect, by means of several techniques such as STM and Scanning Electron Microscopy with Polarization Analysis (SEMPA)<sup>64,65</sup>. The latter consists in that, given some conventional electron source, the beam can be initially polarized or polarized emitted by the source. This polarization is visualized as a selection process which filters

electrons in one spin state in preference to the other, in this case with a strong dependence on the spin-orbit coupling effect.

Eq.2.19 allows us to obtain a degree, or percentage, of polarization as long as the ISO coupling is not considered. For this case, as we take into account the ISO coupling, the measured polarization is interpreted as being weighted by the spin-dependent transmission probabilities, so we resort to the formula used by Worledge et al.<sup>66</sup>, which is shown in equation 2.20.

$$P_z = \frac{|F_\uparrow|^2 - |F_\downarrow|^2}{|F_\uparrow|^2 + |F_\downarrow|^2}, \quad (2.20)$$

where  $F_\uparrow$  and  $F_\downarrow$  represent the transmitted amplitudes shown in Eq.2.14, corresponding to spin up and down, respectively.

## 2.7 Electron Transport Computations

Charge current is the flow of electric charge through a material, due to the movement of electrons inside it<sup>67</sup>. For this case, it is the flow of charge, caused by the movement of electrons, that crosses the potential barrier. Its spin is not considered, only the charge (see Fig.2.10). In quantum mechanics it can be described in terms of a velocity operator, giving it a physical sense. This can be calculated with its respective formula,

$$J_Q = \psi^\dagger(\mathbf{r})\hat{v}_x\psi(\mathbf{r}), \quad (2.21)$$

where,  $\psi(\mathbf{r})$  is the wavefunction of the electrons with respect to its position and  $\hat{v}_x$  is different for the regions, due to is equal  $\hat{v}_x = \partial H/\partial p_x$ .

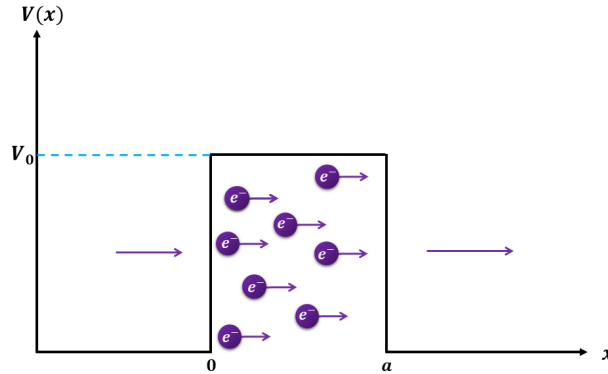


Figure 2.10: The charge current consists of the flow of electrons through the potential barrier.

Spin current refers to the flow of spin from one part of a material to another, as the figure 2.11 shows. In the ideal situation where spin is conserved, it is simply defined as the difference between the electron currents in the two

spin states. Therefore, physically, it has been usual to define this current as the expected value of the product of the spin and velocity observable<sup>68</sup>. However, when SO coupling exists, as mentioned above, the spin is not conserved.

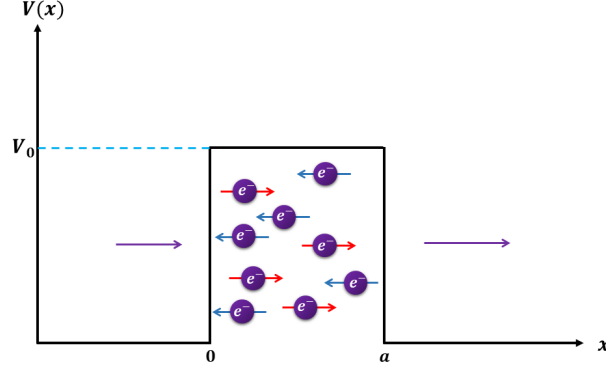


Figure 2.11: Scheme of the Spin Current. Electrons with different spin states flow from left to right through the potential barrier.

The spin current that is discussed in this work is polarized in the direction parallel to the one-dimensional plane that is considered for the tunneling process, and therefore to the length of the DNA molecule. It is possible to derive a continuity equation, based on a general quantum mechanical principle, that relates the densities of spin, current and torque as shown,

$$\frac{\partial S_z}{\partial t} + \nabla \cdot \mathbf{J}_s = \mathcal{T}_z, \quad (2.22)$$

where  $S_z$  is the spin density for a particle in a (spinor) state,  $\mathcal{T}_z$  is the torque density and  $\mathbf{J}_s$  is the spin current.

The spin current density here is given by the conventional definition:

$$\mathbf{J}_s = \text{Re} \psi^\dagger(\mathbf{r}) \frac{1}{2} \{ \hat{\mathbf{v}}, \hat{\mathbf{s}}_z \} \psi(\mathbf{r}), \quad (2.23)$$

where  $\hat{\mathbf{v}}$  is the velocity operator, and  $\{, \}$  denotes the anticommutator. These definitions can be easily restated in a manybody language by regarding the wave functions as field operators and by taking the expectation value in the quantum state of the system. The presence of the torque density  $\mathcal{T}_z$  reflects the fact that spin is not conserved microscopically in systems with spin-orbit coupling<sup>68</sup>.

For reasons of symmetry, sometimes the average torque vanishes for the bulk of the system, i.e.,  $(1/V) \int dV \mathcal{T}_z(\mathbf{r}) = 0$ . This is applicable for any sample with inversion symmetry, however, when we want a particular component of the spin it could disappear in the bulk on average. For this case, where the average spin torque density vanishes in the bulk, the torque density can be written as a divergence of a torque dipole density,

$$\mathcal{T}_z(\mathbf{r}) = -\nabla \cdot \mathbf{P}_\tau(\mathbf{r}). \quad (2.24)$$

Moving it to the left-hand side of 2.22:

$$\frac{\partial S_z}{\partial t} + \nabla \cdot (\mathbf{J}_s + \mathbf{P}_\tau) = 0. \quad (2.25)$$

This is in the form of the standard sourceless continuity equation, and shows that the spin is conserved on average in such systems. The corresponding transport current will be:

$$\mathcal{J}_s = \mathbf{J}_s + \mathbf{P}_\tau. \quad (2.26)$$

There is still an arbitrariness in defining the effective spin current because Eq.2.24 does not uniquely determine the torque dipole density  $\mathbf{P}_\tau$  from the corresponding torque density  $\mathcal{T}_z$ . In order to eliminate this ambiguity, a physical restriction can be imposed that the torque dipole density is a property of the material that should vanish outside of the sample<sup>68</sup>. Which means that,

$$\int dV \mathbf{P}_\tau = - \int dV \mathbf{r} \nabla \cdot \mathbf{P}_\tau = \int dV \mathbf{r} \mathcal{T}_z(\mathbf{r}). \quad (2.27)$$

Therefore, the effective spin current density, upon bulk average, can be written in the form of:

$$\mathcal{J}_s = \text{Re} \psi^\dagger(\mathbf{r}) \hat{\mathcal{J}}_s \psi(\mathbf{r}), \quad (2.28)$$

where,

$$\hat{\mathcal{J}}_s = \frac{d(\hat{\mathbf{r}} \hat{s}_z)}{dt}, \quad (2.29)$$

is the Effective Spin Current Operator. In the development of this equation, the term  $\hat{\mathbf{r}}(d\hat{s}_z/dt)$  appears, which is important in our model, since it considers the contribution of the spin torque. So that, developing the definition of the conserved spin current, is obtained:

$$\begin{aligned} \mathcal{J}_s &= \hat{\mathbf{r}} \frac{d\hat{s}_z}{dt} + \frac{d\hat{\mathbf{r}}}{dt} \hat{s}_z, \\ &= \frac{1}{i\hbar} \left( \hat{\mathbf{r}} [\hat{s}_z, \hat{H}] + [\hat{\mathbf{r}}, \hat{H}] \hat{s}_z \right), \\ &= \hat{\mathbf{J}}_s + \hat{\mathbf{P}}_\tau, \end{aligned} \quad (2.30)$$

where  $\hat{H}$  is the Hamiltonian of the system and  $\hat{s}_z$  is the spin operator for the  $z$  component.

### 2.7.1 Spin Torque Density

The spin torque density is used to refer to the change in the state of magnetization induced by spin polarized currents (see Fig.2.12). When ferromagnetic components are incorporated into a device, or molecule in this case, the flowing electrons can become polarized. Due to the spin-based interactions between ferromagnets and electrons, the orientations of the magnetization of ferromagnetic elements can determine the amount of current flow. Through

these same interactions, the spins of the electrons can also influence the orientations of the magnetizations<sup>69</sup>. Which causes a torsion in the spin to adapt to the prevailing orientation.

According to Shi et al.<sup>68</sup>, the torque density can be then computed by the relation:

$$\mathcal{T}_z = Re\psi^\dagger(\mathbf{r})\hat{\tau}\psi(\mathbf{r}), \quad (2.31)$$

where  $\psi(\mathbf{r})$  is the wavefunction of the electrons with respect to its position, and,

$$\begin{aligned} \hat{\tau} &= \frac{d\hat{s}_z}{dt}, \\ &= \frac{1}{i\hbar} [\hat{s}_z, \hat{H}]. \end{aligned} \quad (2.32)$$

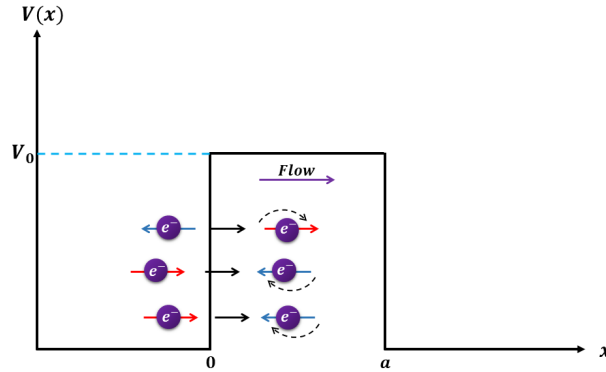


Figure 2.12: Scheme of the Spin Torque. The electrons injected with a spin state, upon entering the potential barrier, undergo a torque force, changing their state.

## 2.8 The Decimation Method

The quantum transport of electrons in Oligoacenes molecules is studied, using the "Decimation" technique. This technique allows a complete description of the electronic structure by reducing the problem of many sites to only two centers, the first and the last of the system, which are separated by many bridge atoms<sup>70</sup>.

Decimation begins with the Hamiltonian of the system derived from the Tight-Binding model, which is naturally associated with linear combination of atomic orbitals (LCAO)<sup>9</sup>. The Tight-Binding Hamiltonian has the general form:

$$\hat{H} = \begin{pmatrix} \ddots & \ddots & & & \\ & E_{n-1} & V_{n-1,n} & 0 & \\ & V_{n,n-1} & E_n & V_{n,n+1} & \\ & 0 & V_{n+1,n} & E_{n+1} & \ddots \\ & & & & \ddots \end{pmatrix} \quad (2.33)$$

where  $E_n$  represents the local potential energy and corresponds to any of the specific atomic orbitals used for each atom and  $V$  represents the interaction between atoms and its nearest neighbors.

The decimation model and process was explained by Pastawski et al. in 1990<sup>70</sup>, the Hamiltonian model described above is used to solve the typical eigenvalue problem  $(\varepsilon \mathbf{1} - \mathbf{H})\mathbf{u} = 0$ . In this model, when obtaining the system equations, this set of linear equations is gradually reduced to just two, that is, the sites of the system are decimated. There are many situations in which physics and chemistry indicate that this is a physically significant model<sup>9</sup>. By performing these operations, it is observed a progressive solution is being built, in which new terms are introduced that indicate that the presence of other sites has the effect of changing or dividing the energies of the site being observed. As a result of these repetitive operations in the system of equations, the procedure of elimination of variables is very general and can exhaust the degrees of freedom of the finite system. Then, it is possible to deduce a recursive scheme to define the parameters that are obtained, which are used to decimate until the two sites that are obtained at the end. These sites will now have self-energies and between them there will now be effective interaction, which are represented by  $\tilde{\mathbf{E}}_1$ ,  $\tilde{\mathbf{E}}_n$  and  $\tilde{\mathbf{V}}_{1,n}$ ,  $\tilde{\mathbf{V}}_{n,1}$  respectively, where  $n$  is the number of the last site in the system.

The decimation method can also be used in two-dimensional systems, therefore also in organic molecules such as oligoacenes. In general, for a two-dimensional system, a "layer by layer" elimination is performed, where each site now represents a layer and becomes an  $n \times n$ -matrix in which the sites of that layer and their interactions are found. Therefore, the parameters obtained in the decimation will also be matrix. A scheme of the decimation procedure in this type of system made by Patawski and Medina is shown in figure 2.13.

Considering the aforementioned scheme, the general equations for the new self-energies are:

$$\tilde{\mathbf{E}}_1 = \mathbf{E}_1 + \Delta_{1(N-1)}^+, \quad (2.34)$$

and

$$\tilde{\mathbf{E}}_N = \mathbf{E}_N + \Delta_N^-. \quad (2.35)$$

These self-energies represent the layer by layer elimination, from 1 to (N-1). Below are the parameters used in this iterative process,

$$\Delta_{1(n)}^+(\varepsilon) = \Delta_{1(n-1)}^+ + \tilde{\mathbf{V}}_{1,n} \frac{1}{\varepsilon \mathbf{1} - \mathbf{E}_n - \Delta_n^-} \tilde{\mathbf{V}}_{n,1}, \quad (2.36)$$

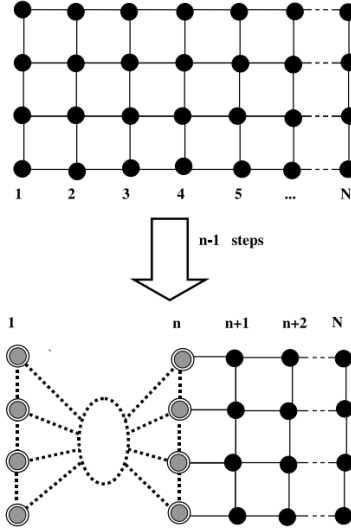


Figure 2.13: H. M. Patawski, and E. Medina. *Scheme of the decimation of a finite tight-binding strip. As the elimination of intermediate layers proceeds the effective site energies and interaction appears.* 2001. Retrieved from<sup>9</sup>.

$$\Delta_{n+1}^-(\varepsilon) = \tilde{\mathbf{V}}_{n+1,n} \frac{1}{\varepsilon \mathbf{1} - \mathbf{E}_n - \Delta_n^-} \tilde{\mathbf{V}}_{n,n+1}, \quad (2.37)$$

$$\tilde{\mathbf{V}}_{1,n+1} = \tilde{\mathbf{V}}_{1,n} \frac{1}{\varepsilon \mathbf{1} - \mathbf{E}_n - \Delta_n^-} \mathbf{V}_{n,n+1} + \mathbf{V}_{1,n+1}, \quad (2.38)$$

with the initial values:

$$\begin{aligned} \Delta_{1(1)}^+(\varepsilon) &= 0, \\ \Delta_2^-(\varepsilon) &= 0, \\ \tilde{\mathbf{V}}_{1,2} &= \mathbf{V}_{1,2}. \end{aligned} \quad (2.39)$$

where  $\Delta_{1(n)}^+(\varepsilon)$  is the self-energy correction to the 1<sup>st</sup> layer when all layers (to the right) including the  $n^{\text{th}}$  have been eliminated,  $\Delta_{n+1}^-(\varepsilon)$  is the self-energy correction to layer  $(n+1)$  when layers to the left have been eliminated and  $\tilde{\mathbf{V}}_{1,n+1}$  is the effective interaction between layers<sup>9,70</sup>. Consequently, it is clearly seen that the method procedure described above can be used in molecular systems such as oligoacenes.

# Chapter 3

## Results & Discussion

### 3.1 Spin-Orbit Interaction and Spin Selectivity for Tunneling Electron Transfer in DNA\*

#### 3.1.1 Tight-Binding Hamiltonian

In order to derive the analytical model of DNA was necessary to use a molecular Hamiltonian based on an analytical Tight-Binding model, which was derived by Varela et al<sup>7</sup>. In this case, only the kinetic terms and Spin-Orbit Spin-Orbit (SO) coupling of atoms involved in  $\pi$  orbitals are considered, due to the SO interaction is active only in one strain on the DNA molecule. The Hamiltonian is:

$$H = (\epsilon_{2p}^{\pi} + 2tf(k))\mathbf{1}_s - 2g(k)\lambda_{SO}s_y, \quad (3.1)$$

where  $\mathbf{1}_s$  represents the unit matrices in spin space,  $\lambda_{SO}$  is the SO coupling parameter and  $t$  the hopping parameter that depend on explicit structural parameters of the molecule, as shown in section 2.4. In the model used here, we considered explicitly the role of the Hydrogen bonds between bases in DNA on the SO coupling<sup>71</sup>. Taking the radius, the pitch of the DNA-helix, and the angle between two consecutive bases equal to  $a = 1.18$  nm,  $b = 3.4$  nm and  $\Delta\phi = \pi/5$ , respectively, the estimated parameters for the kinetic energy terms  $t = 10$  meV and for the SO interaction  $\lambda_{SO} = 3.6$  to 20 meV.

It is important to remember  $f(k)$  and  $g(k)$  are the functions of reciprocal space of this system, and are defined by,

$$\begin{aligned} f(k) &= \cos(\mathbf{k} \cdot \mathbf{R}), \\ g(k) &= \sin(\mathbf{k} \cdot \mathbf{R}), \end{aligned} \quad (3.2)$$

where the wavevector  $\mathbf{k}$  can be written in terms of only two components  $\mathbf{k} = (k_y, k_x)$ .

---

\*“Effective spin-orbit couplings in an analytical tight-binding model of DNA: Spin filtering and chiral spin transport”, *Phys. Rev. B* **2016**, 93.

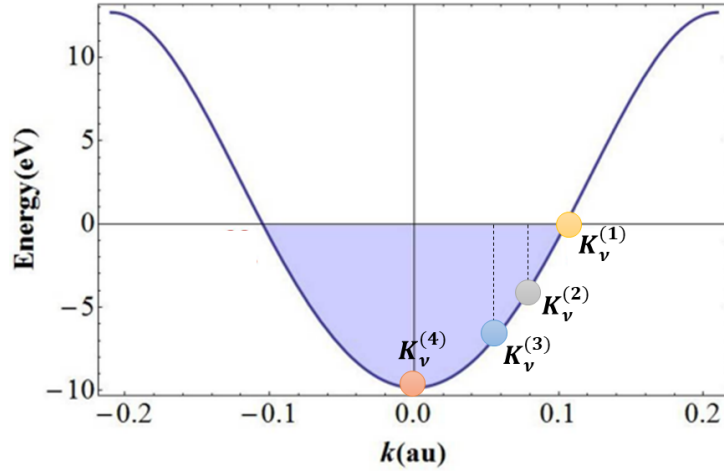


Figure 3.1: Energy spectrum in the first zone of Brillouin. The points  $K_\nu$  at which the expansion was performed are shown. Retrieved and adapted from<sup>7</sup>

This model contemplates a half-filled orbital per base (modeled by carbon atoms, with the mobile electron on  $p_z$  orbital), while the  $p_x$  and  $p_y$  orbitals are bonded on the bases of DNA; therefore, the Fermi level for one orbital per base would be half full (figure 3.1). However, the transfer of charge or doping by the substrate on which the molecule is bound determines the dispersion ratio around the Fermi energy. This can modify the charge and thus shift the dispersion from the inflection point  $K_\nu$  for the kinetic energy term, and  $K_\nu$  is written in terms of the lattice parameter  $R$ , with  $\nu = \pm 1$ . With this in mind, the Fermi energy is set at various points  $K_\nu$ , and a small perturbative doping in the vicinity of the Fermi level is produced, such that  $k = K_\nu + q$ . The values for  $K$  used are those shown in Table 3.1,

Inflection Points	Value
$K_\nu^{(1)}$	$\left(\nu \frac{\pi}{2R}, 0\right)$
$K_\nu^{(2)}$	$\left(\nu \frac{3\pi}{4R}, 0\right)$
$K_\nu^{(3)}$	$\left(\nu \frac{\pi}{4R}, 0\right)$
$K_\nu^{(4)}$	$(0, 0)$

Table 3.1: Inflection points  $K_\nu$  used to apply a small perturbation

The functions  $f(\mathbf{k})$  and  $g(\mathbf{k})$  are expanded to the lowest order in  $q$ , making the approximation  $\mathbf{k} \cdot \mathbf{R} \ll 1$ . For our interest, we pick the expansion around point  $K_\nu^{(4)} = (0, 0)$ , getting:

$$\begin{aligned}
 f(k) &= \cos[(q+0)R] = \cos(qR) \\
 &= 1 - \frac{q^2 R^2}{2} + \mathcal{O}(q^4) \dots,
 \end{aligned} \tag{3.3}$$

and

$$\begin{aligned} g(k) &= \sin[(q+0)R] = \sin(qR) \\ &= qR + \mathcal{O}(q^3)\dots, \end{aligned} \quad (3.4)$$

Using the above expressions and substituting in eq.3.1, the resulting Hamiltonian is:

$$H = \left[ \varepsilon_{2p}^\pi + 2t \left( 1 - \frac{q^2 R^2}{2} \right) \right] \mathbf{1}_s - 2qR\lambda_{SO} s_y. \quad (3.5)$$

The Hamiltonian, to lowest order in  $q$ , show a quadratic dispersion for the kinetic term and a linear dispersion for the SO term, This is important, due to it establishes the possibility of reversing temporal reversion without having problems with the Hamiltonian, since there is no problem in the sense that the electron moves, in addition by having a linear dispersion in the SO term it is established there is an asymmetry, that is, a spin separation, which is necessary to have spin selectivity.

According to the  $k \cdot p$  theory, we can requantize this Hamiltonian to address the problem of tunneling in the vicinity of Fermi level<sup>72</sup>:  $q \rightarrow -i\partial_x$  and  $-\hbar^2/2R^2|t| \rightarrow m$ . So, the obtained Hamiltonian, eliminating constant terms, is:

$$H = \frac{1}{2m} (-i\hbar\partial_x)^2 \mathbf{1} + \alpha\sigma_y(-i\hbar\partial_x) \quad (3.6)$$

where  $\alpha = -\frac{2R}{\hbar}\lambda_{SO}$  and  $\sigma_y$  is the Pauli matrix. It should be noted that this Hamiltonian derived with our model is the same as obtained in reference<sup>73</sup>, so we can use it to study the CISS effect by tunneling.

### 3.1.2 Potential Barrier

The previous Hamiltonian is presented in an analytical model to describe the transfer of electrons under a potential barrier with ISO interaction. We assume electrons are injected from a localized donor state and received at an acceptor site. The electrons interact with a potential barrier of height  $V_0$  and width  $a$ , in which the ISO interaction is active, as shown in figure 3.2<sup>74</sup>. This model considers an incident state of momentum  $p_x$  and energy  $E$  consistent with the donor ground state ( $i\hbar\partial_x = p_x$ ), where  $x$  found along the tangent of the helix. Then, the Hamiltonian for the scattering problem will be:

$$H = \begin{cases} \left( \frac{p_x^2}{2m} + V_o \right) \mathbf{1} + \alpha\sigma_y p_x & ; \quad 0 \leq x \leq a \\ \text{donor/accept. states} & ; \quad \text{outside.} \end{cases} \quad (3.7)$$

This Hamiltonian acts on spinors  $\psi$  with the form:

$$\psi(x) = \begin{pmatrix} \psi_\uparrow(x) \\ \psi_\downarrow(x) \end{pmatrix} \quad (3.8)$$

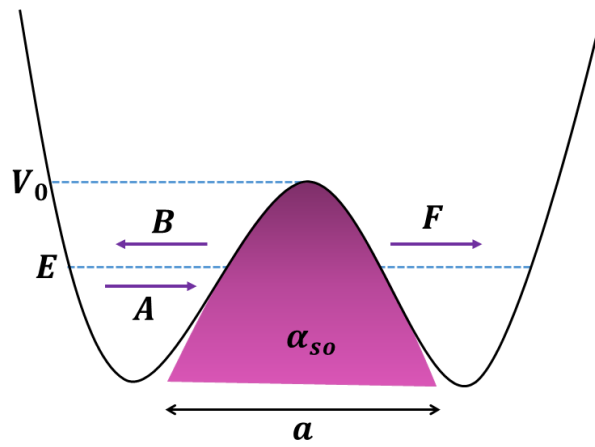


Figure 3.2: Scattering potential barrier model with SO interaction, where  $E$  is the energy of the incident electron and  $V_0$  is the barrier potential. The labels corresponding to the amplitudes of the wave functions of incidence ( $A$ ), reflected ( $B$ ) and transmitted ( $F$ ) are shown. The ISO interaction is just active on the barrier.

where the arrows indicate the up, down spin-components. Then, in the general solution, the spinor for the incident beam is:

$$\psi_{in}(x) = \begin{pmatrix} A_{\uparrow} \\ A_{\downarrow} \end{pmatrix} e^{ikx}, \quad (3.9)$$

and the scattered beam is given by the spinor:

$$\psi_{out}(x) = \begin{pmatrix} F_{\uparrow} \\ F_{\downarrow} \end{pmatrix} e^{ikx}. \quad (3.10)$$

Next, expressions for the wave vectors are derived, solving the eigenvalues problem for each of the regions.

Considering an incident electron with energy  $E$  and wave vector  $k$ , the general solutions are:

$$\psi_{\text{I}} = \begin{pmatrix} A_{\uparrow} \\ A_{\downarrow} \end{pmatrix} e^{ik_1 x} + \begin{pmatrix} B_{\uparrow} \\ B_{\downarrow} \end{pmatrix} e^{-ik_1 x}, \quad x \leq 0, \quad (3.11)$$

$$\psi_{\text{III}} = \begin{pmatrix} F_{\uparrow} \\ F_{\downarrow} \end{pmatrix} e^{ikx} \quad ; \quad x \geq a, \quad (3.12)$$

where  $A$ ,  $B$  and  $F$  are the amplitudes of the wave function, incident, reflected and transmitted, respectively. For the region of the barrier, the solution when  $E > V_0$  is:

$$\psi_{\text{II}} = \begin{pmatrix} C_{\uparrow} e^{iq_1 x} \\ C_{\downarrow} e^{iq_1 x} \end{pmatrix} + \begin{pmatrix} D_{\uparrow} e^{-iq_1 x} \\ D_{\downarrow} e^{-iq_1 x} \end{pmatrix}; \quad 0 \leq x \leq a, \quad (3.13)$$

and, for  $E < V_0$ :

$$\psi_{II} = \begin{pmatrix} C_{\uparrow} e^{q_1 x} \\ C_{\downarrow} e^{q_1 x} \end{pmatrix} + \begin{pmatrix} D_{\uparrow} e^{-q_1 x} \\ D_{\downarrow} e^{-q_1 x} \end{pmatrix}; \quad 0 \leq x \leq a, \quad (3.14)$$

where  $C$  and  $D$  are the amplitudes inside barrier region.

For Region I, using the corresponding Hamiltonian in Eq.3.7 and the particular solution in Eq.3.11.

$$\begin{pmatrix} \frac{p_x^2}{2m} & 0 \\ 0 & \frac{p_x^2}{2m} \end{pmatrix} \begin{bmatrix} \begin{pmatrix} A_{\uparrow} \\ A_{\downarrow} \end{pmatrix} e^{ik_1 x} + \begin{pmatrix} B_{\uparrow} \\ B_{\downarrow} \end{pmatrix} e^{-ik_1 x} \end{bmatrix} = E \begin{bmatrix} \begin{pmatrix} A_{\uparrow} \\ A_{\downarrow} \end{pmatrix} e^{ik_1 x} + \begin{pmatrix} B_{\uparrow} \\ B_{\downarrow} \end{pmatrix} e^{-ik_1 x} \end{bmatrix}, \quad (3.15)$$

a system of two differential equations is obtained:

$$-\frac{\hbar^2}{2m} (A_{\uparrow} \partial_x^2 e^{ik_1 x} + B_{\uparrow} \partial_x^2 e^{-ik_1 x}) = E (A_{\uparrow} e^{ik_1 x} + B_{\uparrow} e^{-ik_1 x}), \quad (3.16)$$

$$-\frac{\hbar^2}{2m} (A_{\downarrow} \partial_x^2 e^{ik_1 x} + B_{\downarrow} \partial_x^2 e^{-ik_1 x}) = E (A_{\downarrow} e^{ik_1 x} + B_{\downarrow} e^{-ik_1 x}). \quad (3.17)$$

For the spin up, the Eq.3.16 was employed:

$$-\frac{\hbar^2}{2m} [A_{\uparrow} (-k^2) e^{ik_1 x} + B_{\uparrow} (-k^2) e^{-ik_1 x}] = E (A_{\uparrow} e^{ik_1 x} + B_{\uparrow} e^{-ik_1 x}), \quad (3.18)$$

$$\frac{\hbar^2 k^2}{2m} (A_{\uparrow} e^{ik_1 x} + B_{\uparrow} e^{-ik_1 x}) = E (A_{\uparrow} e^{ik_1 x} + B_{\uparrow} e^{-ik_1 x}). \quad (3.19)$$

So, then:

$$k_1 = \frac{\sqrt{2mE}}{\hbar}, \quad (3.20)$$

and the process for the spin down is the same and, so, the same result.

For Region III, taking into consideration the Hamiltonian of Eq. 3.7 and the particular solution for this region in Eq. 3.12:

$$\begin{pmatrix} \frac{p_x^2}{2m} & 0 \\ 0 & \frac{p_x^2}{2m} \end{pmatrix} \begin{bmatrix} \begin{pmatrix} F_{\uparrow} \\ F_{\downarrow} \end{pmatrix} e^{ikx} \end{bmatrix} = E \begin{bmatrix} \begin{pmatrix} F_{\uparrow} \\ F_{\downarrow} \end{pmatrix} e^{ikx} \end{bmatrix}. \quad (3.21)$$

Solving the above system, two differential equations are getting:

$$-\frac{\hbar^2}{2m} (F_{\uparrow} \partial_x^2 e^{ik_1 x}) = E (F_{\uparrow} e^{ik_1 x}), \quad (3.22)$$

$$-\frac{\hbar^2}{2m} (F_{\downarrow} \partial_x^2 e^{ik_1 x}) = E (F_{\downarrow} e^{ik_1 x}). \quad (3.23)$$

For the spin up, the Eq.3.22 was employed:

$$-\frac{\hbar^2}{2m} [F_{\uparrow} (-k^2) e^{ik_1 x}] = E (F_{\uparrow} e^{ik_1 x}), \quad (3.24)$$

$$\frac{\hbar^2 k^2}{2m} (F_{\uparrow} e^{ik_1 x}) = E (F_{\uparrow} e^{ik_1 x}) \quad (3.25)$$

So, then:

$$\frac{\hbar^2 k^2}{2m} = E \quad (3.26)$$

$$k_3 = \frac{\sqrt{2mE}}{\hbar}. \quad (3.27)$$

The process for the spin down is the same and, so, the same result.

We will obtain the wave vector  $q_s$  for the region II, in which we have a dependence on the orientation of the spin.

### Energies Above Barrier $E > V_0$

Using the corresponding Hamiltonian to within the region of the potential barrier in the Eq.3.7 and the particular solution of Eq. 3.13:

$$\begin{pmatrix} \frac{p_x^2}{2m} + V_o & -i\alpha p_x \\ i\alpha p_x & \frac{p_x^2}{2m} + V_o \end{pmatrix} \left[ \begin{pmatrix} C_{\uparrow} e^{iq_1 x} \\ C_{\downarrow} e^{iq_1 x} \end{pmatrix} + \begin{pmatrix} D_{\uparrow} e^{-iq_1 x} \\ D_{\downarrow} e^{-iq_1 x} \end{pmatrix} \right] = E \left[ \begin{pmatrix} C_{\uparrow} e^{iq_1 x} \\ C_{\downarrow} e^{iq_1 x} \end{pmatrix} + \begin{pmatrix} D_{\uparrow} e^{-iq_1 x} \\ D_{\downarrow} e^{-iq_1 x} \end{pmatrix} \right]. \quad (3.28)$$

Solving the above system, a system of two differential equations is obtained:

$$\left( -\frac{\hbar^2}{2m} \partial_x^2 + V_o \right) (C_{\uparrow} e^{iq_1 x} + D_{\uparrow} e^{-iq_1 x}) - \alpha \hbar \partial_x (C_{\downarrow} e^{iq_1 x} + D_{\downarrow} e^{-iq_1 x}) = E (C_{\uparrow} e^{iq_1 x} + D_{\uparrow} e^{-iq_1 x}), \quad (3.29)$$

$$\left( -\frac{\hbar^2}{2m} \partial_x^2 + V_o \right) (C_{\downarrow} e^{iq_1 x} + D_{\downarrow} e^{-iq_1 x}) + \alpha \hbar \partial_x (C_{\uparrow} e^{iq_1 x} + D_{\uparrow} e^{-iq_1 x}) = E (C_{\downarrow} e^{iq_1 x} + D_{\downarrow} e^{-iq_1 x}). \quad (3.30)$$

Then, the equations 3.29 and 3.30 will be:

$$\left( \frac{\hbar^2 q^2}{2m} + V_o - E \right) (C_{\uparrow} e^{iqx} + D_{\uparrow} e^{-iqx}) - i\alpha \hbar q (C_{\downarrow} e^{iqx} - D_{\downarrow} e^{-iqx}) = 0, \quad (3.31)$$

$$i\alpha \hbar q (C_{\uparrow} e^{iqx} - D_{\uparrow} e^{-iqx}) + \left( \frac{\hbar^2 q^2}{2m} + V_o - E \right) (C_{\downarrow} e^{iqx} + D_{\downarrow} e^{-iqx}) = 0. \quad (3.32)$$

In order to solve this system of equations to find the wave vector  $q$ , we can reduce it using only one amplitude for both spin states, so a new system of equations is obtained as follows:

$$\left( \frac{\hbar^2 q^2}{2m} + V_o - E \right) C_{\uparrow} - i\alpha \hbar q C_{\downarrow} = 0, \quad (3.33)$$

$$i\alpha \hbar q C_{\uparrow} + \left( \frac{\hbar^2 q^2}{2m} + V_o - E \right) C_{\downarrow} = 0. \quad (3.34)$$

This is equivalent to the following matrix system:

$$\begin{pmatrix} \frac{\hbar^2 q^2}{2m} + V_o - E & -i\alpha\hbar q \\ i\alpha\hbar q & \frac{\hbar^2 q^2}{2m} + V_o - E \end{pmatrix} \begin{pmatrix} C_\uparrow \\ C_\downarrow \end{pmatrix} = \begin{pmatrix} 0 \\ 0 \end{pmatrix}, \quad (3.35)$$

and the solution can be obtained by matching the matrix determinant to 0,

$$\begin{vmatrix} \frac{\hbar^2 q^2}{2m} + V_o - E & -i\alpha\hbar q \\ i\alpha\hbar q & \frac{\hbar^2 q^2}{2m} + V_o - E \end{vmatrix} = 0, \quad (3.36)$$

such that,

$$\left[ \frac{\hbar^2}{2m} (q^2 + q_0^2) - E \right]^2 - (\alpha\hbar q)^2 = 0, \quad (3.37)$$

Where  $q_0^2 = \frac{2mV_0}{\hbar^2}$ . Then,

$$E_\pm = \frac{\hbar^2}{2m} (q^2 + q_0^2) \mp \alpha\hbar q = \frac{\hbar^2 k^2}{2m}, \quad (3.38)$$

$$q^2 \mp \frac{2m\alpha}{\hbar} q + q_0^2 - k^2 = 0. \quad (3.39)$$

Finally, the wave vector is:

$$q_s = \pm \sqrt{k^2 - q_0^2 + \left(\frac{m\alpha}{\hbar}\right)^2} + s \left(\frac{m\alpha}{\hbar}\right), \quad (3.40)$$

where  $s$  is the label associated with the spin up(down) such that  $s = +(-)$ . In the previous expression we can clearly see the dependence of the wave vector  $q$  with the spin  $s$ , the potential of the barrier  $V_0$  and with the magnitude of the ISO interaction,  $\alpha$ . It is important to note that, when the incident energy is greater than the potential of the barrier, the wave vector in this region is always real and the amplitudes will oscillate due to the standing wave patterns between the edges of the barrier and the spin precession due to Intrinsic Spin-Orbit (ISO) coupling.

### Energies below the barrier $E < V_o$

Using the corresponding Hamiltonian to within the region of the potential barrier in the Eq.3.7 and the particular solution of Eq. 3.14:

$$\begin{pmatrix} \frac{p_x^2}{2m} + V_o & -i\alpha p_x \\ i\alpha p_x & \frac{p_x^2}{2m} + V_o \end{pmatrix} \left[ \begin{pmatrix} C_\uparrow e^{q_\uparrow x} \\ C_\downarrow e^{q_\downarrow x} \end{pmatrix} + \begin{pmatrix} D_\uparrow e^{-q_\uparrow x} \\ D_\downarrow e^{-q_\downarrow x} \end{pmatrix} \right] = E \left[ \begin{pmatrix} C_\uparrow e^{q_\uparrow x} \\ C_\downarrow e^{q_\downarrow x} \end{pmatrix} + \begin{pmatrix} D_\uparrow e^{-q_\uparrow x} \\ D_\downarrow e^{-q_\downarrow x} \end{pmatrix} \right]. \quad (3.41)$$

Solving the above system, a system of two differential equations is obtained:

$$\left( -\frac{\hbar^2}{2m} \partial_x^2 + V_o \right) (C_\uparrow e^{q_\uparrow x} + D_\uparrow e^{-q_\uparrow x}) - \alpha\hbar \partial_x (C_\downarrow e^{q_\downarrow x} + D_\downarrow e^{-q_\downarrow x}) = E (C_\uparrow e^{q_\uparrow x} + D_\uparrow e^{-q_\uparrow x}), \quad (3.42)$$

$$\left( -\frac{\hbar^2}{2m} \partial_x^2 + V_o \right) (C_\downarrow e^{q_\downarrow x} + D_\downarrow e^{-q_\downarrow x}) + \alpha\hbar \partial_x (C_\uparrow e^{q_\uparrow x} + D_\uparrow e^{-q_\uparrow x}) = E (C_\downarrow e^{q_\downarrow x} + D_\downarrow e^{-q_\downarrow x}). \quad (3.43)$$

Then, the equations 3.42 and 3.43 will be:

$$\left(-\frac{\hbar^2 q^2}{2m} + V_o - E\right)(C_\uparrow e^{qx} + D_\uparrow e^{-qx}) - \alpha\hbar q(C_\downarrow e^{qx} + D_\downarrow e^{-qx}) = 0, \quad (3.44)$$

$$\alpha\hbar q(C_\uparrow e^{qx} + D_\uparrow e^{-qx}) + \left(-\frac{\hbar^2 q^2}{2m} + V_o - E\right)(C_\downarrow e^{qx} + D_\downarrow e^{-qx}) = 0. \quad (3.45)$$

As was done in the previous case ( $E > V_0$ ), in order to result this system of equations to find the wave vector  $q$ , we focus on an amplitude for both spin states. So, a new system of equation was obtained.

$$\left(-\frac{\hbar^2 q^2}{2m} + V_o - E\right)C_\uparrow - \alpha\hbar q C_\downarrow = 0, \quad (3.46)$$

$$\alpha\hbar q C_\uparrow + \left(-\frac{\hbar^2 q^2}{2m} + V_o - E\right)C_\downarrow = 0. \quad (3.47)$$

This is equivalent to the following matrix system:

$$\begin{pmatrix} -\frac{\hbar^2 q^2}{2m} + V_o - E & -\alpha\hbar q \\ \alpha\hbar q & -\frac{\hbar^2 q^2}{2m} + V_o - E \end{pmatrix} \begin{pmatrix} C_\uparrow \\ C_\downarrow \end{pmatrix} = \begin{pmatrix} 0 \\ 0 \end{pmatrix}, \quad (3.48)$$

and the solution can be obtained by

$$\begin{vmatrix} -\frac{\hbar^2 q^2}{2m} + V_o - E & -\alpha\hbar q \\ \alpha\hbar q & -\frac{\hbar^2 q^2}{2m} + V_o - E \end{vmatrix} = 0, \quad (3.49)$$

or

$$\left[\frac{\hbar^2}{2m}(q_0^2 - q^2) - E\right]^2 + (\alpha\hbar q)^2 = 0, \quad (3.50)$$

where  $q_0^2 = \frac{2mV_0}{\hbar^2}$ . Then,

$$E_\pm = \frac{\hbar^2}{2m}(q_0^2 - q^2) \pm i\alpha\hbar q = \frac{\hbar^2 k^2}{2m}, \quad (3.51)$$

$$q^2 \mp i\frac{2m\alpha}{\hbar}q + k^2 - q_0^2 = 0. \quad (3.52)$$

Finally, the wave vector is:

$$q_s = \pm \sqrt{q_0^2 - k^2 - \left(\frac{m\alpha}{\hbar}\right)^2} + is\left(\frac{m\alpha}{\hbar}\right), \quad (3.53)$$

where  $s$  is the label associated with the spin up(down) such that  $s = +(-)$ . This case is the most interesting in this work, since having the incident energy below the barrier the tunneling process occurs. Transmission below the barrier presents three physical scenarios, which depend on the interaction between three energies: the incident energy of the electron  $E$ , the height of the barrier  $V_0$  and the energy corresponding to the ISO coupling. For this, we analyze the above equation (3.53) of the wave vector  $q_s$  inside the barrier:

- $\alpha = 0$ ,  $q_s = \sqrt{|q_0^2 - k^2|}$ , there is no spin activity for this case, therefore a simple decay in the wave function is expected.
- $|q_0^2 - k^2| > (m\alpha/\hbar)^2$ , and if  $\alpha \neq 0$ , then the wavevector  $q_s$  will be a complex number. So, we have an underdamped decay of the barrier wavefunction.
- $|q_0^2 - k^2| < (m\alpha/\hbar)^2$ , later the wavevector  $q_s$  is purely imaginary number. Hence, the wave function into the barrier region is a plane wave.

### Eigenfunctions Coefficients

In order to observe the wave behavior of the electrons in the three regions, it is necessary to find the amplitudes of the wave functions. For this, the edge conditions are applied, in which the following equations are obtained:

- For  $\psi_I(x=0) = \psi_{II}(x=0)$ ,

$$A_s + B_s = C_s + D_s, \quad (3.54)$$

- For  $\partial_x \psi_I(x=0) = \partial_x \psi_{II}(x=0)$ ,

$$\frac{k}{q_s}(A_s - B_s) = C_s - D_s, \quad (3.55)$$

- For  $\psi_{II}(x=a) = \psi_{III}(x=a)$ ,

$$C_s e^{iq_s a} + D_s e^{-iq_s a} = F_s e^{ika}, \quad (3.56)$$

- For  $\partial_x \psi_{II}(x=a) = \partial_x \psi_{III}(x=a)$ ,

$$C_s e^{iq_s a} - D_s e^{-iq_s a} = \frac{k}{q_s} F_s e^{ika}. \quad (3.57)$$

The coefficients of the wave functions can be derived in terms of the amplitude of the incident wave  $A_s$ , solving the system of equations.

The figure 3.3 shows how, when the electrons collide with the barrier, one spin component is almost purely exponential while the other oscillates below the barrier, for some values of the scattering parameters. This results in spin polarization through this ISO coupling tunneling process. The values used are those shown in the table 3.2.

Parameter	Value
$a$	5 nm
$k$	0.44 nm <sup>-1</sup>
$q_0$	0.446 nm <sup>-1</sup>
$m\alpha^2/2$	80 meV

Table 3.2: Parameters of the spin components probability  $\psi^2$ .

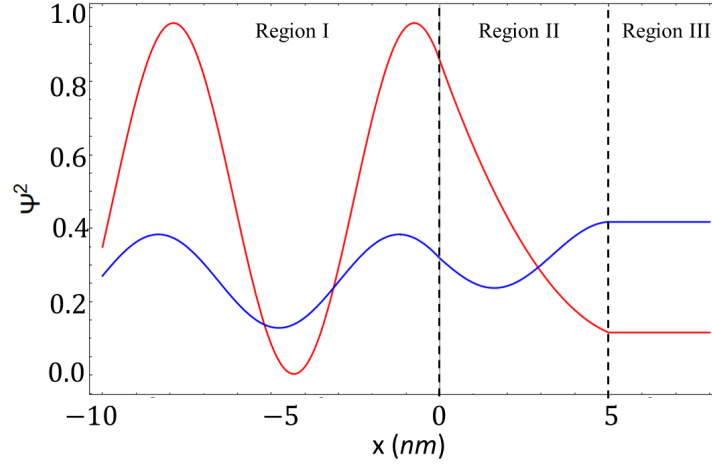


Figure 3.3: Spin components probability with energy values near to the barrier potential. A favorable behavior towards a spin component is observed within the barrier, causing a spin polarization.

## 3.2 Spin Polarization

The potential barrier model is introduced, in which the electrons are injected from a donor site to a acceptor site passing through the barrier with a lower energy than the potential of the barrier. The polarization effect suffered by the spins of the electrons at different incidence energies is observed and analyzed.

Some studies, in which tunneling has been reported using DNA as a bridge in donor-bridge-acceptor (D-B-A) systems, report barriers of width  $10 - 40 \text{ \AA}$ <sup>75</sup>. Additionally, the voltage difference in the DNA is also reported, that is, the height of the barrier, with values between  $0.5 - 2 \text{ eV}$ <sup>76,77</sup>. Therefore, the value of  $q_0 = 7.24 \text{ nm}^{-1}$  corresponding to an energy of the potential barrier of  $V = 2 \text{ eV}$ , is estimated for various values of  $k$ .

Figure 3.4 shows a polarization diagram in which  $k = 7 \text{ nm}^{-1}$ , corresponding to an incidence energy of  $E = 1.87 \text{ eV}$ , that is, with an energy very close to the height of the barrier. This energy allows to obtain a high polarization of approximately 60% is achieved. Polarization increases as SO interaction do it, as expected. Furthermore, there is an important relationship between the polarization and the width of the barrier, since higher polarization is observed when the width of the barrier increases, from 1 nm to 3 nm polarization values are high.

Then, a value of  $k = 5 \text{ nm}^{-1}$  was used, this value corresponds to an incidence energy  $E = 1 \text{ eV}$ , that is, that the wave would be half the height of the potential barrier. The scheme for these values are shown in figure 3.5. In this regime it is observed that the polarization decreases, now a polarization of 50% is obtained, in addition, in a similar way to the previous case, there is a greater polarization when the width of the barrier increases. However, it is observed that now the range, with respect to the width of the barrier, for a higher polarization decreases, now it is observed that it goes from 0.3 nm, unlike the previous one that was from 1 nm.

Figure 3.6 depicted the polarization when the value of the incident energy of the wave is well below the height

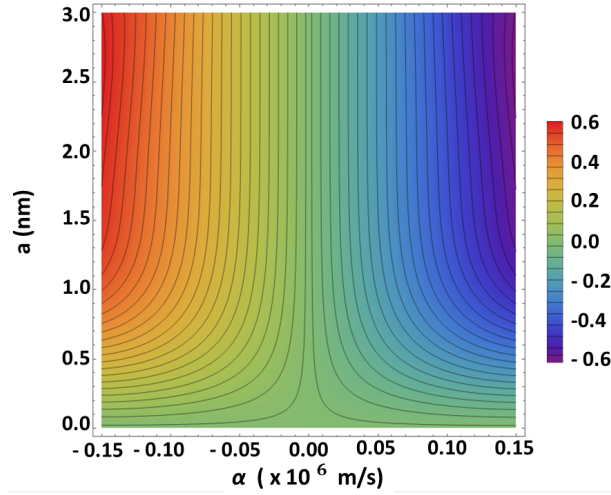


Figure 3.4: Spin asymmetry  $P_z$  as a function of  $a$  in nm and the velocity of the SO interaction in m/s. The values for the incident wave function  $k = 7 \text{ nm}^{-1}$  and the barrier height  $q_0 = 7.24 \text{ nm}^{-1}$  are fixed.

of the barrier, that is, when the regime is deep within the barrier, with  $k = 3.6 \text{ nm}^{-1}$  and  $k = 1 \text{ nm}^{-1}$ , corresponding to incident energy  $E = 0.5 \text{ eV}$  and  $E = 0.03 \text{ eV}$  respectively. As the incident energy goes below the barrier the magnitude of the polarization decreases as the maximum is now approximately 30%. Furthermore, the range with respect to the width of the barrier decreases, when  $k = 3.6 \text{ nm}^{-1}$  a greater polarization is observed between  $0.04 \text{ nm} - 0.2 \text{ nm}$ , while for  $k = 1 \text{ nm}^{-1}$ , the deepest, the high polarization is observed between  $0.02 \text{ nm} - 0.07 \text{ nm}$ .

The polarization images of the different regimes of the barrier demonstrate that a high polarization can be achieved, of a magnitude of up to 60%, but the polarization decreases when the incidence energy approaches the bottom of the barrier, that is to say when  $k$  is smaller. The closer the wave is to the height of the barrier the magnitude of polarization will be higher, this could be because one spin component sees the barrier higher than the other and produces the tunneling effect.

Thanks to these observations, the width parameter of the barrier can be manipulated by stretching the DNA molecule to achieve the one necessary to obtain a high magnitude of polarization. Something interesting is observed in the graphs, as  $k$  becomes smaller, there is a range in which a high polarization with respect to the width of the barrier is observed, however, for  $a$  greater than a certain value, the polarization decreases exponentially. This affirms the results obtained in ref<sup>78</sup> about mechanical deformations in DNA. When the molecule undergoes a stretching deformation, the SO interaction increases exponentially, but it has a maximum, in which, from that point, the SO coupling decreases until it is equal to zero. This phenomenon occurs because at this point the pitch is very large compared to the radius of the helix so the SO interaction is weakened since the overlaps depend on the inverse of the separation of the DNA bases. Therefore, the molecule can be stretched to obtain a large magnitude of polarization, but only up to a point, since after the maximum, the polarization decreases, as observed in our graphs.

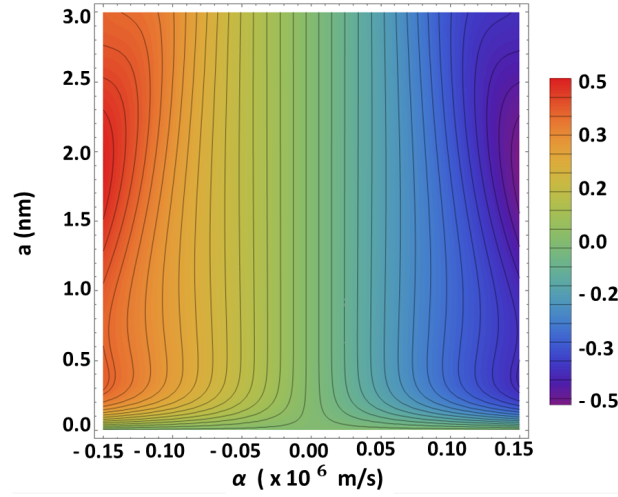


Figure 3.5: Spin asymmetry  $P_z$  as a function of  $a$  in nm and the velocity of the SO interaction in m/s. The values for the incident wave function  $k = 5 \text{ nm}^{-1}$  and the barrier height  $q_0 = 7.24 \text{ nm}^{-1}$  are fixed.

### 3.3 Charge Current.

The charge current can be calculated with its respective formula,

$$J_Q = \psi^\dagger \hat{v}_x \psi, \quad (3.58)$$

where  $\hat{v}_x$  is different for the regions, due to is equal  $\hat{v}_x = \partial H / \partial p_x$ . So, the velocity in regions 1 and 3 will be:

$$\hat{v}_{x,I} = \hat{v}_{x,III} = \begin{pmatrix} p_x/m & 0 \\ 0 & p_x/m \end{pmatrix}, \quad (3.59)$$

and in region 2:

$$\hat{v}_{x,II} = \begin{pmatrix} p_x/m & -i\alpha \\ i\alpha & p_x/m \end{pmatrix}, \quad (3.60)$$

#### 3.3.1 Region I

Now, using:

$$\psi_I = \begin{pmatrix} A_\uparrow \\ A_\downarrow \end{pmatrix} e^{ik_1 x} + \begin{pmatrix} B_\uparrow \\ B_\downarrow \end{pmatrix} e^{-ik_1 x}; \quad x \leq 0, \quad (3.61)$$

First, we calculate  $\hat{v}_x \psi_I$ :

$$\hat{v}_x \psi_I = \begin{pmatrix} p_x/m & 0 \\ 0 & p_x/m \end{pmatrix} \begin{pmatrix} A_\uparrow e^{ik_1 x} + B_\uparrow e^{-ik_1 x} \\ A_\downarrow e^{ik_1 x} + B_\downarrow e^{-ik_1 x} \end{pmatrix}, \quad (3.62)$$

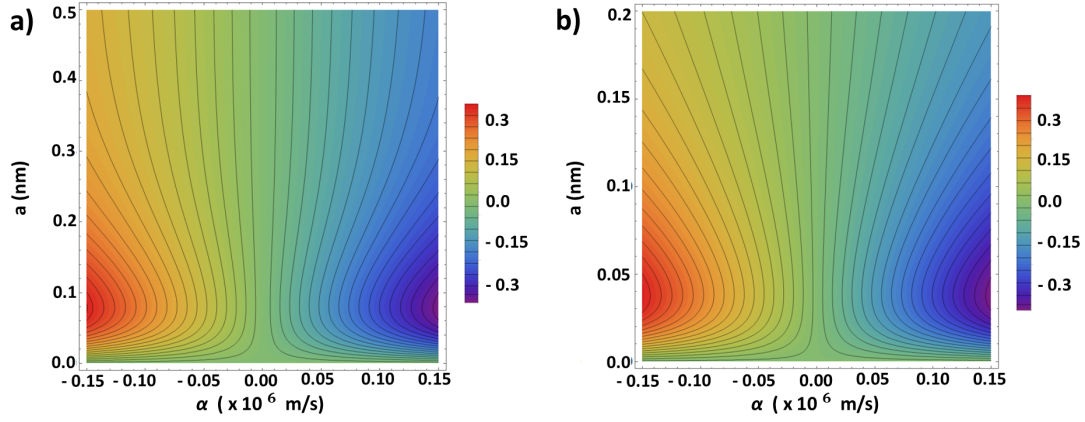


Figure 3.6: Spin asymmetry  $P_z$  as a function of  $a$  in nm and the velocity of the SO interaction in m/s with the barrier height  $q_0 = 7.24 \text{ nm}^{-1}$ . a) The values for the incident wave function  $k = 2 \text{ nm}^{-1}$ . b) The values for the incident wave function  $k = 1 \text{ nm}^{-1}$ .

Hence, we can calculate the charge current:

$$J_Q^I = \psi_I^\dagger \hat{v}_x \psi_I = \begin{pmatrix} A_\uparrow^* e^{-ik_1 x} + B_\uparrow^* e^{ik_1 x}, & A_\downarrow^* e^{-ik_1 x} + B_\downarrow^* e^{ik_1 x} \end{pmatrix} * \begin{pmatrix} \frac{\hbar k_1}{m} (A_\uparrow e^{ik_1 x} - B_\uparrow e^{-ik_1 x}) \\ \frac{\hbar k_1}{m} (A_\downarrow e^{ik_1 x} - B_\downarrow e^{-ik_1 x}) \end{pmatrix}, \quad (3.63)$$

or

$$J_Q^I = \frac{\hbar k_1}{m} (|A_\uparrow|^2 + |A_\downarrow|^2 - |B_\uparrow|^2 - |B_\downarrow|^2 - A_\uparrow^* B_\uparrow e^{-2ik_1 x} - A_\downarrow^* B_\downarrow e^{-2ik_1 x} + A_\uparrow B_\uparrow^* e^{2ik_1 x} + A_\downarrow B_\downarrow^* e^{2ik_1 x}), \quad (3.64)$$

Finally, using complex function properties:

$$J_Q^I = \frac{\hbar k_1}{m} (|A_\uparrow|^2 + |A_\downarrow|^2 - |B_\uparrow|^2 - |B_\downarrow|^2 - 2i \text{Im}(A_\uparrow^* B_\uparrow e^{-2ik_1 x}) - 2i \text{Im}(A_\downarrow^* B_\downarrow e^{-2ik_1 x})). \quad (3.65)$$

### 3.3.2 Region II

Using the corresponding  $\hat{v}_x$  for this region in the Eq.3.60 the charging current was calculated for both cases,  $E > V_0$  and  $E < V_0$

**Above barrier energies  $E > V_0$**

$$\psi_{II} = \begin{pmatrix} C_\uparrow \\ C_\downarrow \end{pmatrix} e^{iq_s x} + \begin{pmatrix} D_\uparrow \\ D_\downarrow \end{pmatrix} e^{-iq_s x}. \quad (3.66)$$

In the same way as in region 1,  $\hat{v}_x \psi_{II}$  was calculated first:

$$\hat{v}_x \psi_{II} = \begin{pmatrix} p_x/m & -i\alpha \\ i\alpha & p_x/m \end{pmatrix} \begin{pmatrix} C_\uparrow e^{iq_1 x} + D_\uparrow e^{-iq_1 x} \\ C_\downarrow e^{iq_1 x} + D_\downarrow e^{-iq_1 x} \end{pmatrix}, \quad (3.67)$$

then, we obtained the following expression:

$$\hat{v}_x \psi_{II} = \left( \begin{array}{c} -\frac{i\hbar}{m} (iq_\uparrow C_\uparrow e^{iq_\uparrow x} - iq_\uparrow D_\uparrow e^{-iq_\uparrow x}) - i\alpha (C_\downarrow e^{iq_\downarrow x} + D_\downarrow e^{-iq_\downarrow x}) \\ i\alpha (C_\uparrow e^{iq_\uparrow x} + D_\uparrow e^{-iq_\uparrow x}) - \frac{i\hbar}{m} (iq_\downarrow C_\downarrow e^{iq_\downarrow x} - iq_\downarrow D_\downarrow e^{-iq_\downarrow x}) \end{array} \right), \quad (3.68)$$

Next, the charging current is:

$$\begin{aligned} J_Q^II &= \frac{\hbar q_\uparrow}{m} (|C_\uparrow|^2 e^{-i(q_\uparrow^* - q_\uparrow)x} - |D_\uparrow|^2 e^{i(q_\uparrow^* - q_\uparrow)x} + C_\uparrow D_\uparrow^* e^{i(q_\uparrow^* + q_\uparrow)x} - C_\uparrow^* D_\uparrow e^{-i(q_\uparrow^* + q_\uparrow)x}) \\ &\quad - i\alpha (C_\uparrow^* C_\downarrow e^{-i(q_\uparrow^* - q_\downarrow)x} + D_\uparrow^* D_\downarrow e^{i(q_\uparrow^* - q_\downarrow)x} + C_\uparrow^* D_\downarrow e^{-i(q_\uparrow^* + q_\downarrow)x} + C_\downarrow D_\uparrow^* e^{i(q_\uparrow^* + q_\downarrow)x}) \\ &\quad + \frac{\hbar q_\downarrow}{m} (|C_\downarrow|^2 e^{-i(q_\downarrow^* - q_\downarrow)x} - |D_\downarrow|^2 e^{i(q_\downarrow^* - q_\downarrow)x} - C_\downarrow^* D_\downarrow e^{-i(q_\downarrow^* + q_\downarrow)x} + C_\downarrow D_\downarrow^* e^{i(q_\downarrow^* + q_\downarrow)x}) \\ &\quad + i\alpha (C_\uparrow C_\downarrow^* e^{-i(q_\uparrow^* - q_\downarrow)x} + D_\uparrow D_\downarrow^* e^{i(q_\uparrow^* - q_\downarrow)x} + C_\downarrow D_\uparrow e^{-i(q_\downarrow^* + q_\uparrow)x} + C_\uparrow D_\downarrow^* e^{i(q_\downarrow^* + q_\uparrow)x}), \end{aligned} \quad (3.69)$$

or:

$$\begin{aligned} J_Q^II &= \frac{\hbar q_\uparrow}{m} (|C_\uparrow|^2 e^{-2\text{Im}(q_\uparrow)x} - |D_\uparrow|^2 e^{2\text{Im}(q_\uparrow)x}) + \frac{\hbar q_\downarrow}{m} (|C_\downarrow|^2 e^{-2\text{Im}(q_\downarrow)x} - |D_\downarrow|^2 e^{2\text{Im}(q_\downarrow)x}) \\ &\quad + \frac{\hbar q_\uparrow}{m} 2i \text{Im}(C_\uparrow D_\uparrow^* e^{2i \text{Re}(q_\uparrow)x}) + \frac{\hbar q_\downarrow}{m} 2i \text{Im}(C_\downarrow D_\downarrow^* e^{2i \text{Re}(q_\downarrow)x}) + i\alpha (2i \text{Im}(C_\uparrow C_\downarrow^* e^{-i(q_\uparrow^* - q_\downarrow)x}) + 2i \text{Im}(D_\uparrow D_\downarrow^* e^{-i(q_\uparrow^* - q_\downarrow)x}) \\ &\quad + 2i \text{Im}(C_\uparrow D_\downarrow e^{-i(q_\uparrow^* + q_\downarrow)x}) + 2i \text{Im}(C_\downarrow D_\uparrow e^{i(q_\downarrow^* + q_\uparrow)x}). \end{aligned} \quad (3.70)$$

### Energies below the barrier $E < V_0$

For this case was necessary to use the Eq. 3.60 the corresponding wave equation 3.14 and its conjugate:

$$\psi_{II}^\dagger = \left( C_\uparrow^* e^{-q_\uparrow^* x} + D_\uparrow^* e^{q_\uparrow^* x}, C_\downarrow^* e^{-q_\downarrow^* x} + D_\downarrow^* e^{q_\downarrow^* x} \right). \quad (3.71)$$

First,  $\hat{v}_x \psi_{II}$  was calculated.

$$\begin{aligned} \hat{v}_x \psi_{II} &= \left( \begin{array}{cc} p_x/m & -i\alpha \\ i\alpha & p_x/m \end{array} \right) \left( \begin{array}{c} C_\uparrow e^{q_\uparrow x} + D_\uparrow e^{-q_\uparrow x} \\ C_\downarrow e^{q_\downarrow x} + D_\downarrow e^{-q_\downarrow x} \end{array} \right) \\ &= \left( \begin{array}{c} -\frac{i\hbar q_\uparrow}{m} (C_\uparrow e^{q_\uparrow x} - D_\uparrow e^{-q_\uparrow x}) - i\alpha (C_\downarrow e^{q_\downarrow x} + D_\downarrow e^{-q_\downarrow x}) \\ i\alpha (C_\uparrow e^{q_\uparrow x} + D_\uparrow e^{-q_\uparrow x}) - \frac{i\hbar q_\downarrow}{m} (C_\downarrow e^{q_\downarrow x} - D_\downarrow e^{-q_\downarrow x}) \end{array} \right) \end{aligned} \quad (3.72)$$

Then, the expression for charging current is

$$J_Q^II = \psi_{II}^\dagger \hat{v}_x \psi_{II} = \left( C_\uparrow^* e^{-q_\uparrow^* x} + D_\uparrow^* e^{q_\uparrow^* x}, C_\downarrow^* e^{-q_\downarrow^* x} + D_\downarrow^* e^{q_\downarrow^* x} \right) * \left( \begin{array}{c} -\frac{i\hbar q_\uparrow}{m} (C_\uparrow e^{q_\uparrow x} - D_\uparrow e^{-q_\uparrow x}) - i\alpha (C_\downarrow e^{q_\downarrow x} + D_\downarrow e^{-q_\downarrow x}) \\ i\alpha (C_\uparrow e^{q_\uparrow x} + D_\uparrow e^{-q_\uparrow x}) - \frac{i\hbar q_\downarrow}{m} (C_\downarrow e^{q_\downarrow x} - D_\downarrow e^{-q_\downarrow x}) \end{array} \right), \quad (3.73)$$

Finally, using some complex function properties.

$$\begin{aligned}
J_Q^{II} = & -\frac{i\hbar q_\uparrow}{m} \left( |C_\uparrow|^2 e^{2i \operatorname{Im}(q_\uparrow)x} - |D_\uparrow|^2 e^{-2i \operatorname{Im}(q_\uparrow)x} + C_\uparrow D_\uparrow^* e^{2 \operatorname{Re}(q_\uparrow)x} - C_\uparrow^* D_\uparrow e^{-2 \operatorname{Re}(q_\uparrow)x} \right) \\
& - i \frac{\hbar q_\downarrow}{m} \left( |C_\downarrow|^2 e^{2i \operatorname{Im}(q_\downarrow)x} - |D_\downarrow|^2 e^{-2i \operatorname{Im}(q_\downarrow)x} + C_\downarrow D_\downarrow^* e^{2 \operatorname{Re}(q_\downarrow)x} - C_\downarrow^* D_\downarrow e^{-2 \operatorname{Re}(q_\downarrow)x} \right) \\
& - i\alpha \left( C_\uparrow^* C_\downarrow e^{-(q_\uparrow^* - q_\downarrow)x} + D_\uparrow^* D_\downarrow e^{(q_\uparrow^* - q_\downarrow)x} + C_\uparrow^* D_\downarrow e^{-(q_\uparrow^* + q_\downarrow)x} + C_\downarrow D_\uparrow^* e^{(q_\uparrow^* + q_\downarrow)x} \right) \\
& + i\alpha \left( C_\uparrow C_\downarrow^* e^{-(q_\uparrow - q_\downarrow^*)x} + D_\uparrow D_\downarrow^* e^{(q_\uparrow - q_\downarrow^*)x} + C_\uparrow^* D_\uparrow e^{-(q_\uparrow^* + q_\downarrow)x} + C_\downarrow D_\downarrow^* e^{(q_\uparrow^* + q_\downarrow)x} \right).
\end{aligned} \tag{3.74}$$

### 3.3.3 Region III

Taking the respective values for this region.

$$\psi_{III} = \begin{pmatrix} F_\uparrow \\ F_\downarrow \end{pmatrix} e^{ik_3 x}, \tag{3.75}$$

$$\psi_{III} = \begin{pmatrix} F_\uparrow e^{ik_3 x} \\ F_\downarrow e^{ik_3 x} \end{pmatrix}, \tag{3.76}$$

and,

$$\psi_{III}^\dagger = \begin{pmatrix} F_\uparrow^* e^{-ik_3 x} & F_\downarrow^* e^{-ik_3 x} \end{pmatrix}. \tag{3.77}$$

Accordance with wave functions for region 3, the result of the charging current in this region is equal to that of region 1, but changing  $A = F$ ,  $B = 0$  and  $k_1 = k_3$ . So, the final result of charging current is as follows.

$$J_Q^{III} = \frac{\hbar k_3}{m} = (|F_\uparrow|^2 + |F_\downarrow|^2) \tag{3.78}$$

## 3.4 Spin Current

It is possible to calculate the spin current for the region II, that is, the region into the barrier, with the equation:

$$J_s = \operatorname{Re} \psi_{II}^\dagger(\mathbf{r}) \left[ \frac{1}{i\hbar} \left( \hat{r} [\hat{S}_z, H] + [\hat{r}, H] \hat{S}_z \right) \right] \psi_{II}(\mathbf{r}) \tag{3.79}$$

First, using the term  $[\hat{S}_z, H]$  which was previously calculated, the term  $\hat{r}[\hat{S}_z, H]$  was calculated, where  $\hat{r} = x$  in this case

$$[\hat{S}_z, H] = \begin{pmatrix} 0 & -i\hbar\alpha p_x \\ -i\hbar\alpha p_x & 0 \end{pmatrix}, \tag{3.80}$$

and,

$$\hat{r}[\hat{S}_z, H] = \begin{pmatrix} 0 & -ix\hbar\alpha p_x \\ -ix\hbar\alpha p_x & 0 \end{pmatrix}. \tag{3.81}$$

Next the term  $[\hat{r}, H]$  was calculated, then  $[\hat{r}, H]\hat{S}_z$ , and

$$[\hat{S}_z, H] = \hat{r}H - H\hat{r} = \begin{pmatrix} x\left(\frac{p_x^2}{2m} + V_0\right) & -i\alpha p_x \\ i\alpha p_x & x\left(\frac{p_x^2}{2m} + V_0\right) \end{pmatrix} - \begin{pmatrix} \left(\frac{p_x^2}{2m} + V_0\right)x & -i\alpha p_x x \\ i\alpha p_x x & \left(\frac{p_x^2}{2m} + V_0\right) \end{pmatrix} \quad (3.82)$$

$$[\hat{S}_z, H]\hat{S}_z = \frac{\hbar}{2} \begin{pmatrix} x\frac{p_x^2}{2m} & \alpha(ip_x + \hbar) \\ \alpha(ip_x - \hbar) & -x\frac{p_x^2}{2m} \end{pmatrix} \quad (3.83)$$

Finally,

$$\hat{r}[\hat{S}_z, H] + [\hat{r}, H]\hat{S}_z = \frac{\hbar}{2} \begin{pmatrix} x\frac{p_x^2}{2m} & -\alpha(ip_x - \hbar) \\ -\alpha(ip_x + \hbar) & -x\frac{p_x^2}{2m} \end{pmatrix}, \quad (3.84)$$

then,

$$\frac{1}{i\hbar} \left( \hat{r}[\hat{S}_z, H] + [\hat{r}, H]\hat{S}_z \right) = \frac{1}{2i} \begin{pmatrix} x\frac{p_x^2}{2m} & -\alpha(ip_x - \hbar) \\ -\alpha(ip_x + \hbar) & -x\frac{p_x^2}{2m} \end{pmatrix} \quad (3.85)$$

### 3.4.1 Above barrier energies $E > V_0$

In this section, we consider the wave function for the  $E > V_0$ . Now,

$$\left[ \frac{1}{i\hbar} \left( \hat{r}[\hat{S}_z, H] + [\hat{r}, H]\hat{S}_z \right) \right] \psi_{II}(\mathbf{r}) = \frac{1}{2i} \begin{pmatrix} x\frac{p_x^2}{2m} & -\alpha(ip_x - \hbar) \\ -\alpha(ip_x + \hbar) & -x\frac{p_x^2}{2m} \end{pmatrix} \begin{pmatrix} C_{\uparrow} e^{iq_{\uparrow}x} + D_{\uparrow} e^{-iq_{\uparrow}x} \\ C_{\downarrow} e^{iq_{\downarrow}x} + D_{\downarrow} e^{-iq_{\downarrow}x} \end{pmatrix} \quad (3.86)$$

$$= \frac{1}{2i} \begin{pmatrix} x\frac{q_{\uparrow}^2 \hbar^2}{2m} (C_{\uparrow} e^{iq_{\uparrow}x} + D_{\uparrow} e^{-iq_{\uparrow}x}) - i\alpha \hbar x q_{\downarrow} (C_{\downarrow} e^{iq_{\downarrow}x} - D_{\downarrow} e^{-iq_{\downarrow}x}) + \alpha \hbar (C_{\downarrow} e^{iq_{\downarrow}x} + D_{\downarrow} e^{-iq_{\downarrow}x}) \\ -x\frac{q_{\downarrow}^2 \hbar^2}{2m} (C_{\downarrow} e^{iq_{\downarrow}x} + D_{\downarrow} e^{-iq_{\downarrow}x}) - i\alpha \hbar x q_{\uparrow} (C_{\uparrow} e^{iq_{\uparrow}x} - D_{\uparrow} e^{-iq_{\uparrow}x}) - \alpha \hbar (C_{\uparrow} e^{iq_{\uparrow}x} + D_{\uparrow} e^{-iq_{\uparrow}x}) \end{pmatrix} \quad (3.87)$$

Finally, by applying complex function identities, the final expression is obtained.

$$\begin{aligned} J_s = & \frac{1}{2i} \left[ x \frac{q_{\uparrow}^2 \hbar^2}{2m} (|C_{\uparrow}|^2 e^{-2\text{Im}(q_{\uparrow})x} + |D_{\uparrow}|^2 e^{2\text{Im}(q_{\uparrow})x} + 2 \text{Re}(C_{\uparrow} D_{\uparrow}^* e^{2i \text{Re}(q_{\uparrow})x})) \right. \\ & - x \frac{q_{\downarrow}^2 \hbar^2}{2m} (|C_{\downarrow}|^2 e^{-2\text{Im}(q_{\downarrow})x} + |D_{\downarrow}|^2 e^{2\text{Im}(q_{\downarrow})x} + 2 \text{Re}(C_{\downarrow} D_{\downarrow}^* e^{2i \text{Re}(q_{\downarrow})x})) \\ & + \alpha \hbar (2i \text{Im}(C_{\uparrow}^* C_{\downarrow} e^{i(q_{\downarrow} - q_{\uparrow}^*)x}) + 2i \text{Im}(D_{\uparrow}^* D_{\downarrow} e^{-i(q_{\downarrow} - q_{\uparrow}^*)x}) + 2i \text{Im}(C_{\uparrow}^* D_{\downarrow} e^{-i(q_{\downarrow} - q_{\uparrow}^*)x}) + 2i \text{Im}(C_{\downarrow} D_{\uparrow}^* e^{i(q_{\downarrow} - q_{\uparrow}^*)x})) \\ & - i\alpha \hbar q_{\uparrow} (C_{\uparrow} C_{\downarrow}^* e^{i(q_{\uparrow} - q_{\downarrow}^*)x} - D_{\uparrow} D_{\downarrow}^* e^{-i(q_{\uparrow} - q_{\downarrow}^*)x} - C_{\downarrow}^* D_{\uparrow} e^{-i(q_{\uparrow} + q_{\downarrow}^*)x} + C_{\uparrow} D_{\downarrow}^* e^{i(q_{\uparrow} + q_{\downarrow}^*)x}) \\ & \left. - i\alpha \hbar q_{\downarrow} (C_{\uparrow}^* C_{\downarrow} e^{i(q_{\downarrow} - q_{\uparrow}^*)x} - D_{\uparrow}^* D_{\downarrow} e^{-i(q_{\downarrow} - q_{\uparrow}^*)x} - C_{\uparrow}^* D_{\downarrow} e^{-i(q_{\downarrow} + q_{\uparrow}^*)x} + C_{\downarrow} D_{\uparrow}^* e^{i(q_{\downarrow} + q_{\uparrow}^*)x}) \right] \quad (3.88) \end{aligned}$$

### 3.4.2 Energies below the barrier $E < V_0$

For the energy  $E < V_0$ , the expression will be:

$$\begin{aligned}
 J_s &= \psi_{II}^\dagger \left[ \frac{1}{i\hbar} (\hat{r} [\hat{S}_z, H] + [\hat{r}, H] \hat{S}_z) \right] \psi_{II} \\
 &= \begin{pmatrix} C_\uparrow e^{q_1 x} + D_\uparrow e^{-q_1 x} \\ C_\downarrow e^{q_1 x} + D_\downarrow e^{-q_1 x} \end{pmatrix} \left[ \frac{1}{2i} \begin{pmatrix} x \frac{p_x^2}{2m} & -\alpha(ip_x - \hbar) \\ -\alpha(ip_x + \hbar) & -x \frac{p_x^2}{2m} \end{pmatrix} \right] \begin{pmatrix} C_\uparrow^* e^{-q_1^* x} + D_\uparrow^* e^{q_1^* x}, & C_\downarrow^* e^{-q_1^* x} + D_\downarrow^* e^{q_1^* x} \end{pmatrix} \quad (3.89)
 \end{aligned}$$

And, applying complex function identities, the final result was achieved.

$$\begin{aligned}
 J_s &= \frac{1}{2i} \left[ -x \frac{q_1^2 \hbar^2}{2m} (|C_\uparrow|^2 e^{2i\text{Im}(q_1)x} + |D_\uparrow|^2 e^{-2i\text{Im}(q_1)x} + C_\uparrow^* D_\uparrow e^{-2\text{Re}(q_1)x} + C_\uparrow D_\uparrow^* e^{2\text{Re}(q_1)x}) \right. \\
 &\quad + x \frac{q_1^2 \hbar^2}{2m} (|C_\downarrow|^2 e^{2i\text{Im}(q_1)x} + |D_\downarrow|^2 e^{-2i\text{Im}(q_1)x} + C_\downarrow^* D_\downarrow e^{-2\text{Re}(q_1)x} + C_\downarrow D_\downarrow^* e^{2\text{Re}(q_1)x}) \\
 &\quad - x\alpha\hbar q_\uparrow (C_\uparrow C_\downarrow^* e^{(q_1 - q_1^*)x} - D_\uparrow D_\downarrow^* e^{-(q_1 - q_1^*)x} - C_\downarrow D_\uparrow e^{-(q_1 + q_1^*)x} + C_\uparrow D_\downarrow^* e^{(q_1 + q_1^*)x}) \\
 &\quad - x\alpha\hbar q_\downarrow (C_\uparrow^* C_\downarrow e^{(q_1 - q_1^*)x} - D_\uparrow^* D_\downarrow e^{-(q_1 - q_1^*)x} - C_\uparrow^* D_\downarrow e^{-(q_1 + q_1^*)x} + C_\downarrow D_\uparrow^* e^{(q_1 + q_1^*)x}) \\
 &\quad + \alpha\hbar (C_\uparrow^* C_\downarrow e^{(q_1 - q_1^*)x} + D_\uparrow^* D_\downarrow e^{-(q_1 - q_1^*)x} + C_\uparrow^* D_\downarrow e^{-(q_1 + q_1^*)x} + C_\downarrow D_\uparrow^* e^{(q_1 + q_1^*)x}) \\
 &\quad \left. - \alpha\hbar (C_\uparrow C_\downarrow^* e^{(q_1 - q_1^*)x} + D_\uparrow D_\downarrow^* e^{-(q_1 - q_1^*)x} + C_\uparrow D_\downarrow^* e^{(q_1 + q_1^*)x} + C_\downarrow^* D_\uparrow e^{-(q_1 + q_1^*)x}) \right]. \quad (3.90)
 \end{aligned}$$

## 3.5 Torque Density

The expression for the torque density is written as:

$$\boldsymbol{\tau}_z = \text{Re} \left\{ \psi^\dagger(\mathbf{r}) \hat{\tau} \psi(\mathbf{r}), \right\} \quad (3.91)$$

where  $\hat{\tau}$  is the torque operator, which can be written as:

$$\hat{\tau} = \frac{d\hat{S}_z}{dt} = \left( \frac{1}{i\hbar} \right) [\hat{S}_z, H]. \quad (3.92)$$

This term is calculated for region II, that is, the region within the potential barrier, for both cases: when the energy is above the potential and when the energy is below this potential.

First, the torque operator was calculated.

$$\begin{aligned}
 \hat{\tau} &= \frac{1}{i\hbar} (\hat{S}_z H - H \hat{S}_z) \\
 &= \frac{1}{i\hbar} \frac{\hbar}{2} \left[ \begin{pmatrix} 1 & 0 \\ 0 & -1 \end{pmatrix} \begin{pmatrix} \frac{p_x^2}{2m} + V_0 & -i\alpha p_x \\ i\alpha p_x & \frac{p_x^2}{2m} + V_0 \end{pmatrix} - \begin{pmatrix} \frac{p_x^2}{2m} + V_0 & -i\alpha p_x \\ i\alpha p_x & \frac{p_x^2}{2m} + V_0 \end{pmatrix} \begin{pmatrix} 1 & 0 \\ 0 & -1 \end{pmatrix} \right] \\
 &= \frac{1}{2i} \begin{pmatrix} 0 & -2i\alpha p_x \\ -2i\alpha p_x & 0 \end{pmatrix} \\
 &= \begin{pmatrix} 0 & -\alpha p_x \\ -\alpha p_x & 0 \end{pmatrix} \quad (3.93)
 \end{aligned}$$

### 3.5.1 Above energies barrier $E > V_0$

Using the Eq. 3.93 and the particular solution Eq.3.13.

$$\hat{\tau}\psi_{II} = \begin{pmatrix} 0 & -\alpha p_x \\ -\alpha p_x & 0 \end{pmatrix} \begin{pmatrix} C_{\uparrow} e^{iq_{\uparrow}x} + D_{\uparrow} e^{-iq_{\uparrow}x} \\ C_{\downarrow} e^{iq_{\downarrow}x} + D_{\downarrow} e^{-iq_{\downarrow}x} \end{pmatrix} = \begin{pmatrix} i\alpha\hbar\partial_x (C_{\downarrow} e^{iq_{\downarrow}x} + D_{\downarrow} e^{-iq_{\downarrow}x}) \\ i\alpha\hbar\partial_x (C_{\uparrow} e^{iq_{\uparrow}x} + D_{\uparrow} e^{-iq_{\uparrow}x}) \end{pmatrix} = \begin{pmatrix} -\alpha\hbar q_{\downarrow} (C_{\downarrow} e^{iq_{\downarrow}x} + D_{\downarrow} e^{-iq_{\downarrow}x}) \\ -\alpha\hbar q_{\uparrow} (C_{\uparrow} e^{iq_{\uparrow}x} + D_{\uparrow} e^{-iq_{\uparrow}x}) \end{pmatrix}. \quad (3.94)$$

So, the torque density is

$$\tau_z = \begin{pmatrix} C_{\uparrow}^* e^{-iq_{\uparrow}^*x} + D_{\uparrow}^* e^{iq_{\uparrow}^*x}, & C_{\downarrow}^* e^{-iq_{\downarrow}^*x} + D_{\downarrow}^* e^{iq_{\downarrow}^*x} \end{pmatrix} \begin{pmatrix} -\alpha\hbar q_{\downarrow} (C_{\downarrow} e^{iq_{\downarrow}x} + D_{\downarrow} e^{-iq_{\downarrow}x}) \\ -\alpha\hbar q_{\uparrow} (C_{\uparrow} e^{iq_{\uparrow}x} + D_{\uparrow} e^{-iq_{\uparrow}x}) \end{pmatrix}. \quad (3.95)$$

Finally, the torque density will be:

$$\tau_z = [ -\alpha\hbar q_{\downarrow} (C_{\uparrow}^* C_{\downarrow} e^{i(q_{\downarrow}-q_{\uparrow}^*)x} - D_{\uparrow}^* D_{\downarrow} e^{-i(q_{\downarrow}-q_{\uparrow}^*)x} + C_{\downarrow} D_{\uparrow}^* e^{i(q_{\downarrow}+q_{\uparrow}^*)x} - C_{\uparrow}^* D_{\downarrow} e^{-i(q_{\downarrow}+q_{\uparrow}^*)x}) \\ - \alpha\hbar q_{\uparrow} (C_{\uparrow} C_{\downarrow}^* e^{i(q_{\uparrow}-q_{\downarrow}^*)x} - D_{\uparrow} D_{\downarrow}^* e^{-i(q_{\uparrow}-q_{\downarrow}^*)x} + C_{\uparrow} D_{\downarrow}^* e^{i(q_{\uparrow}+q_{\downarrow}^*)x} - C_{\downarrow}^* D_{\uparrow} e^{-i(q_{\uparrow}+q_{\downarrow}^*)x}) ]. \quad (3.96)$$

### 3.5.2 Energies below the barrier $E < V_0$

In a similar way, the torque below the barrier is

$$\hat{\tau}\psi_{II} = \begin{pmatrix} 0 & -\alpha p_x \\ -\alpha p_x & 0 \end{pmatrix} \begin{pmatrix} C_{\uparrow} e^{q_{\uparrow}x} + D_{\uparrow} e^{-q_{\uparrow}x} \\ C_{\downarrow} e^{q_{\downarrow}x} + D_{\downarrow} e^{-q_{\downarrow}x} \end{pmatrix} = \begin{pmatrix} i\alpha\hbar\partial_x (C_{\downarrow} e^{q_{\downarrow}x} + D_{\downarrow} e^{-q_{\downarrow}x}) \\ i\alpha\hbar\partial_x (C_{\uparrow} e^{q_{\uparrow}x} + D_{\uparrow} e^{-q_{\uparrow}x}) \end{pmatrix} = \begin{pmatrix} i\alpha\hbar q_{\downarrow} (C_{\downarrow} e^{q_{\downarrow}x} + D_{\downarrow} e^{-q_{\downarrow}x}) \\ i\alpha\hbar q_{\uparrow} (C_{\uparrow} e^{q_{\uparrow}x} + D_{\uparrow} e^{-q_{\uparrow}x}) \end{pmatrix} \quad (3.97)$$

Finally, the torque density will be:

$$\tau_z = [ i\alpha\hbar q_{\downarrow} (C_{\uparrow}^* C_{\downarrow} e^{(q_{\downarrow}-q_{\uparrow}^*)x} - D_{\uparrow}^* D_{\downarrow} e^{-(q_{\downarrow}-q_{\uparrow}^*)x} + C_{\downarrow} D_{\uparrow}^* e^{(q_{\downarrow}+q_{\uparrow}^*)x} - C_{\uparrow}^* D_{\downarrow} e^{-(q_{\downarrow}+q_{\uparrow}^*)x}) \\ + i\alpha\hbar q_{\uparrow} (C_{\uparrow} C_{\downarrow}^* e^{(q_{\uparrow}-q_{\downarrow}^*)x} - D_{\uparrow} D_{\downarrow}^* e^{-(q_{\uparrow}-q_{\downarrow}^*)x} + C_{\uparrow} D_{\downarrow}^* e^{(q_{\uparrow}+q_{\downarrow}^*)x} - C_{\downarrow}^* D_{\uparrow} e^{-(q_{\uparrow}+q_{\downarrow}^*)x}) ]. \quad (3.98)$$

Figures representing torque density are shown. Using equation 3.91, graphs of torque density behavior were obtained for each spin of this model with respect to the speed of the spin-orbit interaction. The values chosen were the same as those used for the previous section. Figure 3.7 has an incident energy value very close to the value of the height of the potential barrier and it can be seen that, first, there is a regime in which, regardless of the ISO value, there is no torque for Neither spin, approximately  $\alpha = 0.01x10^6$  m/s. However, from this value, there is a torque difference for both spins and the one with the highest value is significant. The spin down suffers a greater torque force than the spin up, so thanks to this effect the spin polarization is given for the chosen values of this graph.

Figure 3.8 shows a graph of the torque when the value of the incident energy,  $k = 5.12 \text{ nm}^{-1}$ , is half the value of the height of the potential barrier,  $q_0 = 7.24 \text{ nm}^{-1}$ . For these values, a torque difference is also observed for the up and down spins, but the torque value is smaller compared to figure 3.7. With this, it can be corroborated what

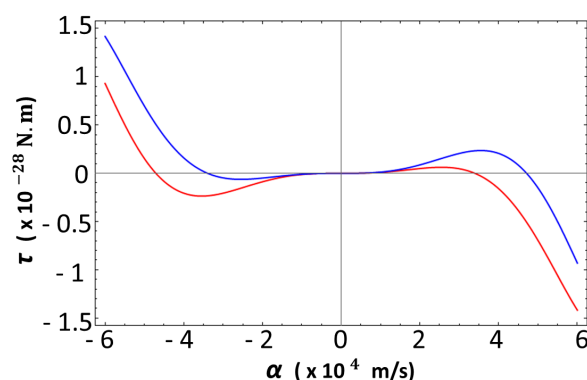


Figure 3.7: Torque Density  $\tau$  in the region II for spin up and down in N.m as a function of the SO interaction in m/s with the incident wave function  $k = 7 \text{ nm}^{-1}$  and the barrier height  $q_0 = 7.24 \text{ nm}^{-1}$

is exposed in the previous section, that as the value of the incident energy is moving away from the height of the barrier, the torque force decreases and therefore the spin polarization as well.

Lastly, a graph of the torque is obtained when the value of the incident energy is well below the value of the height of the barrier,  $k = 1 \text{ nm}^{-1}$ . As expected, the torque force value is very small. Figure 3.9 shows that the torque force produced for these values is in a very low order, so it is practically 0. This shows that when the incident energy of the electron is very low, there is an almost negligible torque force, and therefore there is no significant spin polarization.

According to these obtained graphs, there is a torque force, which is rotated by the spin orbit interaction in the tunneling process. This force causes a spin selectivity, that is, after tunneling there will be a spin that predominates more in the electrons, and therefore a spin polarization is observed, as shown by the polarization graphs presented above. However, it is noted that the torque is relatively large the closer the incident energy of the electron is to the height of the barrier. As the energy is reduced, the torque will also decrease, followed by the polarization, to the extent that neither the torque force nor the spin selectivity occurs at the bottom of the barrier.

### 3.6 S wave Hamiltonian for Oligoacenes: Decimation approach

Peculiar quantum effects manifested in transport properties in molecular systems serve as a basis for interesting quantum device applications. As mentioned in the previous section, chiral molecules with SO coupling in the meV range exhibit spin filtering properties in the absence of time reversal symmetry breaking (Zeeman effects, phase breaking mechanisms). Simple molecules like Oligoacenes<sup>79</sup>, built from concatenating benzene rings is another example of how quantum mechanics can be unintuitive. The conductance as a function of the sequence of increasingly longer molecules in the sequence exhibit first and increase in conductance that then saturates to a relatively constant value independent of length. These results are in contradiction to the expected tunneling to hopping mechanisms expected<sup>77</sup>. This latter behavior is also expected from the polaron picture generally valid in one dimensional systems.

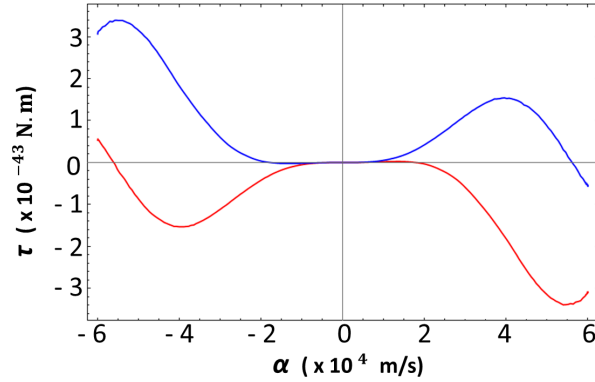


Figure 3.8: Torque Density  $\tau$  in the region II for spin up and down in N.m as a function of the SO interaction in m/s with the incident wave function  $k = 5.12 \text{ nm}^{-1}$  and the barrier height  $q_0 = 7.24 \text{ nm}^{-1}$

To study such quantum effects we propose to approach the problem through analytical minimal models that allow to understand the basic underpinnings of the quantum behavior. What we consider in the following, is such a minimal model, that can be generalized to further detail of the orbitals involved and derive a well defined mechanism that might be involved contradicting the general expectation. It is beyond the scope of our objectives to realize the full scope of this particular project and we will limit the results described here to deriving the minimal Hamiltonians using the decimation technique described in the previous chapter.

We consider the sites of the carbon atoms found in the molecules, which are represented by the circles in figures 3.10 and 3.11. Decimation, the process by which we 'eliminate' sites by introducing their effect on site energies and overlaps, is first performed on a benzene molecule, that is, with a ring. We go from the full Hamiltonian of 6 sites, to a two-site Hamiltonian, as shown in figure 3.10. This process can be understood as an exact renormalization of the 6 site system.

The procedure can be continued to two rings i.e a naphthalene, can be modeled. For this system, we can decimate it to three sites, the first and last with four sites and the middle one with two sites connected by a link. Then, the decimation method is carried out and a two-site system is obtained. The same procedure can be carried out with  $N = 3, 4, 5, 6$ , where  $N$  is the number of rings. First, the complete Hamiltonian was reduced by layers in the same way as before, and finally they were decimated to two places as shown in figure 3.11.

According to the decimation made in the oligoacenes, we observe there is a sequence to follow, both in the full Hamiltonian and in the matrices, when carrying out the decimation procedure starting from Naphthalene, that is, with  $N \geq 2$ . For benzene ( $N = 1$ ), taking into account the interaction between the two paths between the initial and final sites, the full Hamiltonian will be:

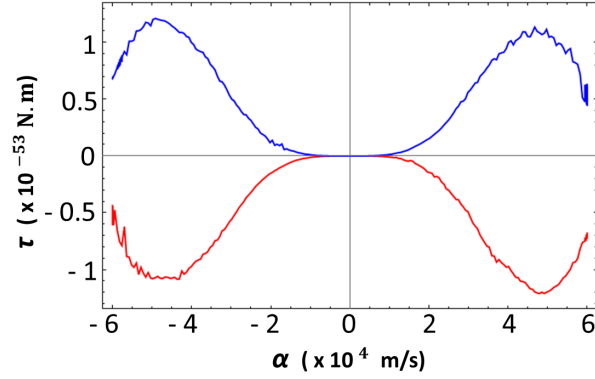


Figure 3.9: Torque Density  $\tau$  in the region II for spin up and down in N.m as a function of the SO interaction in m/s with the incident wave function  $k = 1 \text{ nm}^{-1}$  and the barrier height  $q_0 = 7.24 \text{ nm}^{-1}$

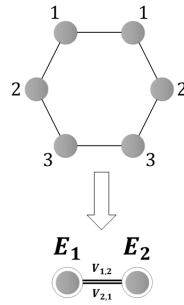


Figure 3.10: Scheme of the decimation method applied to a Benzene molecule.

$$\hat{H} = \sum_{k=1}^M (E_k |k\rangle \langle k|) + \sum_{k=1}^2 (V_{k,k+1} |k\rangle \langle k+1| + V_{k+1,k} |k+1\rangle \langle k|) + \sum_{k=4}^5 (V_{k,k+1} |k\rangle \langle k+1| + V_{k+1,k} |k+1\rangle \langle k|) + V_{1,4} |1\rangle \langle 4| + V_{4,1} |4\rangle \langle 1| + V_{3,6} |3\rangle \langle 6| + V_{6,3} |6\rangle \langle 3| \quad (3.99)$$

where  $M$  is the number of the total sites in the system, i.e., for benzene  $M = 6$ . Therefore, the Hamiltonian for benzene will be a  $6 \times 6$ -matrix. So, the Eq. 3.99 takes the matrix form:

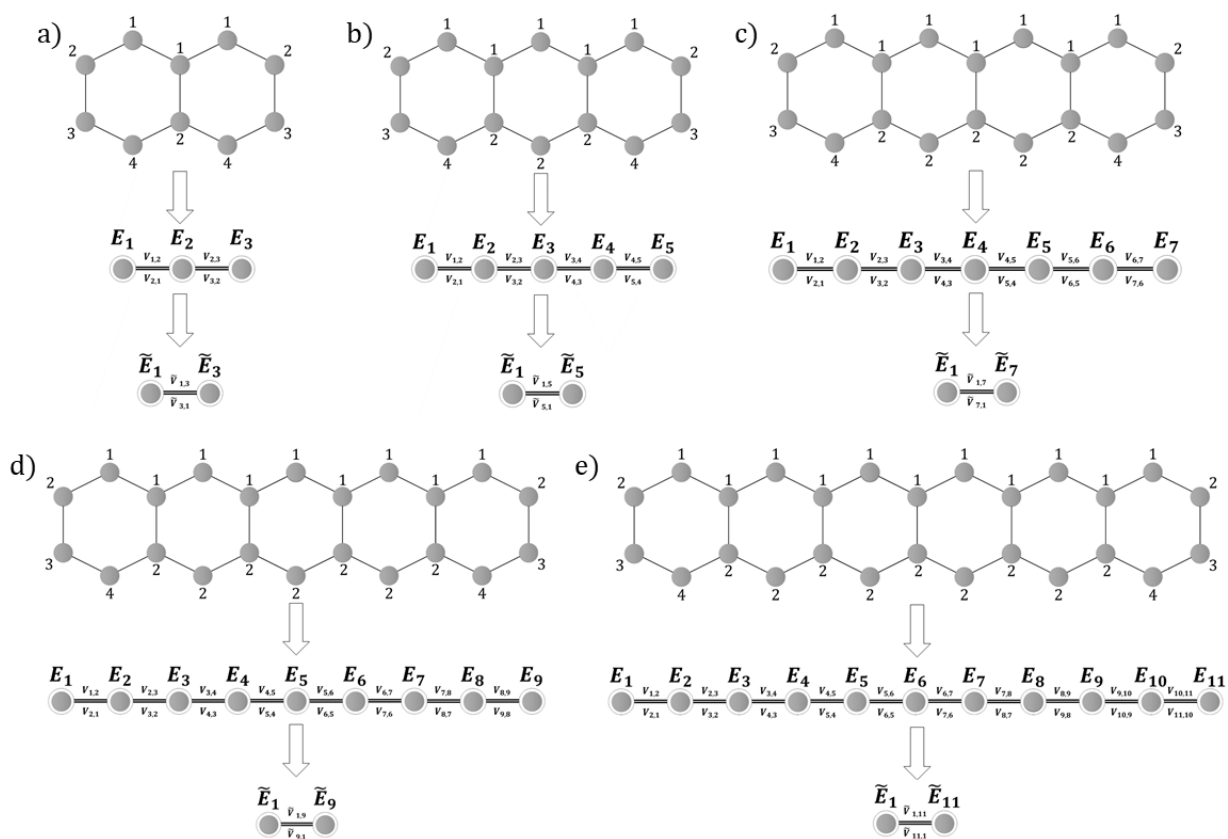


Figure 3.11: Scheme of the decimation method in Oligoacenes. a)Naphthalene, b)Anthracene, c)Tetracene, d)Pentacene, e)Hexacene



Tetracene ( $N = 4$ ). We observed there is a pattern that repeats itself with respect to the interactions  $V$  between the sites by the bonds which connect the rings of the molecule. Consequently, the full Hamiltonian for  $N \geq 2$  can be written as shown in Eq. 3.101.

$$\begin{aligned}
\hat{H} = & \sum_{k=1}^M (E_k |k\rangle \langle k|) + \sum_{k=1}^3 (V_{k,k+1} |k\rangle \langle k+1| + V_{k+1,k} |k+1\rangle \langle k|) \\
& + \sum_{k=M-3}^{M-1} (V_{k,k+1} |k\rangle \langle k+1| + V_{k+1,k} |k+1\rangle \langle k|) \\
& + \sum_{k=0}^{N-2} (V_{5+4(k),6+4(k)} |5+4(k)\rangle \langle 6+4(k)| + V_{6+4(k),5+4(k)} |6+4(k)\rangle \langle 5+4(k)|) \\
& + \sum_{k=4}^{M-5} (V_{k,k+2} |k\rangle \langle k+2| + V_{k+2,k} |k+2\rangle \langle k|) \\
& + V_{1,5} |1\rangle \langle 5| + V_{5,1} |5\rangle \langle 1| + V_{M-4,M} |M-4\rangle \langle M| + V_{M,M-4} |M\rangle \langle M-4|.
\end{aligned} \tag{3.101}$$

As in the case of benzene, the order of the sites is according to the order of the paths and the order of their corresponding sites in each of them. Furthermore, by observing how the number of sites increases as the length of the molecule increases, an equation can be deduced to determine the total number of sites with respect to the number of rings present, which is shown below:

$$M = 6 + 4(N - 1), \tag{3.102}$$

Where  $M$  is the number of all sites in the system and  $N$  is the number of rings in the molecule. In order to make the decimation, each "path" is taken as a matrix  $\mathbf{E}_k$ , which becomes the self-energy of that path with the sites that make it up and their respective interactions. This reduces the Hamiltonian dimension to a  $n \times n$ -matrix that can be written as shown in Eq. 3.103.

$$\hat{H} = \sum_{k=1}^n (\mathbf{E}_k |k\rangle \langle k|) + \sum_{k=1}^{n-1} (\mathbf{V}_{k,k+1} |k\rangle \langle k+1| + \mathbf{V}_{k+1,k} |k+1\rangle \langle k|), \tag{3.103}$$

$$\mathbf{H} = \begin{pmatrix} \mathbf{E}_1 & \mathbf{V}_{1,2} & 0 & \dots & 0 \\ \mathbf{V}_{2,1} & \mathbf{E}_k & \mathbf{V}_{k,k+1} & 0 & \vdots \\ 0 & \mathbf{V}_{k+1,k} & \mathbf{E}_{k+1} & \ddots & 0 \\ \vdots & 0 & \ddots & \ddots & \mathbf{V}_{n-1,n} \\ 0 & \dots & 0 & \mathbf{V}_{n,n-1} & \mathbf{E}_n \end{pmatrix}. \tag{3.104}$$

So, the Eq. 3.103 takes the matrix form shown in Eq. 3.104, where all its elements are matrices and  $n$  is the number of layers considered in the system. The number of layers  $n$  to use in our Hamiltonian is determined from Eq. 3.105

for  $N \geq 2$ , and  $n = 2$  for  $N = 1$ .

$$n = (N \times 2) - 1. \quad (3.105)$$

The matrix elements in the Hamiltonian can be determined by other equations that were derived from the results obtained by the decimation of the oligoacenes while increasing the number of rings in them. Following the scheme in figure 3.11 to determine each "layer" of the molecule, it is obtained that for ( $N \geq 2$ ) the first and last paths always have 4 connected sites, while the intermediate layers have two sites. For  $N = 2$ , which has three paths ( $n = 3$ ), there is only one intermediate path, which represents the union of the two rings of the molecule, so there is an interaction  $V$  between its sites due to the bond which connects them. From this, for each additional ring in the molecule, two layers increase, both with two sites. In one of these layers there is no bond between its two sites, so  $V = 0$  between them. While in the other layer there is a bond connecting its two sites, so there is a coupling  $V$ . In order to write the self-energy matrices for each path, an expression can be written, which is shown in Eq. 3.106, considering the above described about the  $V$  interactions between its sites. Finally, the self-energies of each layer will be  $m \times m$ -matrices, where  $m_k$  is the number of sites in path  $k$ .

The terms  $\mathbf{V}$  are the matrices which represent the interactions between the layers of the system, for example,  $\mathbf{V}_{1,2}$  represents the interaction between path 1 and path 2. These matrices are of size  $m_k \times m_k$ , where the first  $m_k$  is the number of sites of the first layer  $k$  considered, while the second  $m_k$  represents the number of sites in the second layer  $k$  to consider. Therefore, the matrices  $\mathbf{V}_{1,2}$  and  $\mathbf{V}_{2,1}$  will be of size  $4 \times 2$  and  $2 \times 4$  respectively, while  $\mathbf{V}_{n-1,n}$  and  $\mathbf{V}_{n,n-1}$  will be matrices  $2 \times 4$  and  $4 \times 2$  respectively. Additionally, the  $\mathbf{V}$  interactions between the intermediate layers will be  $2 \times 2$ -matrices. Equations 3.107 and 3.108 show a general way to write these matrices.

$$\mathbf{E}_k = \sum_{k=1}^{m_k} (E_k |k\rangle \langle k|) + \sum_{k=1}^{m_k-1} (V_{k,k+1} |k\rangle \langle k+1| + V_{k+1,k} |k+1\rangle \langle k|), \quad (3.106)$$

$$\mathbf{V}_{k,k+1} = V_{1,1} |1\rangle \langle 1| + V_{m_k, m_{k+1}} |m_k\rangle \langle m_{k+1}|, \quad (3.107)$$

$$\mathbf{V}_{k+1,k} = V_{1,1} |1\rangle \langle 1| + V_{m_{k+1}, m_k} |m_{k+1}\rangle \langle m_k|. \quad (3.108)$$

Equations 3.106-3.108 are also valid for the Hamiltonian to be decimated when  $N = 1$ .

Starting from the Hamiltonian of Eq. 3.103 and considering the expressions previously obtained for its matrix elements, the decimation process was carried out to reduce the system to two sites. Therefore, a more simplified Hamiltonian is obtained, which is now a  $2 \times 2$ -matrix, which can be written as Eq. 3.109 and the eigenvalue problem in matrix form is as shown in Eq. 3.110, where  $n$  is the number of paths in the system. The matrix elements of this new Hamiltonian, in which the decimation has already been performed, can be calculated with the expressions described in equations 2.34-2.38. We checked the general decimation procedure described in section 2.8 is applicable to oligoacenes with respect to the number of rings in the molecules.

$$\hat{H} = \tilde{\mathbf{E}}_1 |1\rangle \langle 1| + \tilde{\mathbf{E}}_n |2\rangle \langle 2| + \tilde{\mathbf{V}}_{1,n} |1\rangle \langle 2| + \tilde{\mathbf{V}}_{n,1} |2\rangle \langle 1|, \quad (3.109)$$

$$\begin{pmatrix} \tilde{\mathbf{E}}_1 & \tilde{\mathbf{V}}_{1,n} \\ \tilde{\mathbf{V}}_{n,1} & \tilde{\mathbf{E}}_n \end{pmatrix} \begin{pmatrix} \mathbf{u}_1 \\ \mathbf{u}_n \end{pmatrix} = \varepsilon \mathbf{1} \begin{pmatrix} \mathbf{u}_1 \\ \mathbf{u}_n \end{pmatrix}. \quad (3.110)$$

For example, for a naphthalene molecule, i.e., with  $N = 2$  and, therefore,  $n = 3$ , when performing the decimation process, a problem of eigenvalues is obtained as shown below

$$\begin{pmatrix} \tilde{\mathbf{E}}_1 & \tilde{\mathbf{V}}_{1,3} \\ \tilde{\mathbf{V}}_{3,1} & \tilde{\mathbf{E}}_3 \end{pmatrix} \begin{pmatrix} \mathbf{u}_1 \\ \mathbf{u}_3 \end{pmatrix} = \varepsilon \mathbf{1} \begin{pmatrix} \mathbf{u}_1 \\ \mathbf{u}_3 \end{pmatrix}, \quad (3.111)$$

where, following the general equations of the decimation method

$$\begin{aligned} \hat{\mathbf{E}}_1 &= \mathbf{E}_1 + \Delta_{1(2)}^+ \\ \hat{\mathbf{E}}_3 &= \mathbf{E}_3 + \Delta_3^- \\ \hat{\mathbf{V}}_{1,3} &= \mathbf{V}_{1,2} \frac{1}{\varepsilon_1 - \mathbf{E}_2} \mathbf{V}_{2,3} \\ \hat{\mathbf{V}}_{3,1} &= \mathbf{V}_{3,2} \frac{1}{\varepsilon_1 - \mathbf{E}_2} \mathbf{V}_{2,1}, \end{aligned} \quad (3.112)$$

and

$$\begin{aligned} \Delta_{1(2)}^+ &= \mathbf{V}_{1,2} \frac{1}{\varepsilon_1 - \mathbf{E}_2} \mathbf{V}_{2,1} \\ \Delta_3^- &= \mathbf{V}_{3,2} \frac{1}{\varepsilon_1 - \mathbf{E}_2} \mathbf{V}_{2,3}. \end{aligned} \quad (3.113)$$

It is possible, from this point to enrich the procedures described before to encompass more complicated orbital relations, such as including  $\sigma$  and  $\pi$  structure and internal couplings (not only overlaps). A show of how fruitful this exercise can be is the explanation of the spin activity in helicene<sup>80</sup>. Such projects are left for future work.

## Chapter 4

# Conclusions & Outlook

A theoretical analytical model was developed, which explains, as simply as possible, the spin selectivity that has been experimentally observed in chiral molecules, in this case DNA. From the Hamiltonian derived above, in which we only consider the kinetic energy terms and the ISO coupling, a tunneling process was established by means of a potential barrier with active SOI interaction. The wave vector, when there is tunneling, is dependent on the spin state and can be an imaginary or complex number. Therefore, there is a decay for one of the spin components, while the other oscillates close to the top of the barrier, which is an expected behavior in a system in which spin polarization occurs. Strong spin polarization (up to 60%) is shown in this model for DNA, which is related to the magnitude of the SOI and the width of the barrier. However, the highest magnitude for polarization is observed when the incident energy is close to the height of the barrier. As this energy decreases, polarization is still observed, but at lower magnitudes, especially when it is close to the bottom of the barrier. Additionally, since the polarization is dependent on the SOI and the width of the barrier, a modulation of the polarization is found when these two parameters are varied. This leads us to conclude mechanical deformations can be made to the DNA molecule to increase the magnitude of the ISO interaction and, therefore, the polarization of the system. However, there is a limit in which the SOI coupling decreases by the difference between the radius and the pitch of the helix. Hence, we recover qualitatively the experimental results for mechanical deformations in these systems, with SOI. It is expected that new experimental investigations of mechanical deformations in DNA molecules can be carried out, following our predictions to achieve a desired magnitude of spin polarization.

A model was established to describe and reduce oligoacene molecule systems Hamiltonian by means of the decimation method, which accounts for the structure of these molecules and can be used in future research to analytically study their electronic properties, manifested through transport quantities such as conductance.

The CISS effect can have several applications in industry. The main application of this effect is oriented to the manufacture of information storage devices. Chiral organic molecules, having spin selectivity, can be used for the creation of spin transistors or spin valves. Currently, common transistors, being a semiconductor material, are used in almost all memory devices, such as hard drives, in conjunction with magnetic materials. However, since they are two independent materials, there is a transfer of information between them, which takes time, and a high

energy expenditure by the transistor. This is why the CISS effect opens the possibility of producing devices using chiral molecules instead of ferromagnets, which are complicated and difficult to handle. The advantage will be that information can be read at a much higher resolution, that is, it will be possible to have more information per area in the device, which is important when creating smaller devices in the technological field. As a final result, new devices can be developed that can store more data in less space, faster and more efficient than conventional devices, flexible, with lower energy consumption and using less expensive materials.

Based on the technology mentioned above, it is possible that the CISS effect could have applications in biomedicine. Specifically, it could be used in the manufacture of biosensors, which, for the most part, are used for the detection of different pathologies, such as viruses. Chiral molecules can be used as a transducer component in biosensors, which would lead to the production of faster, more efficient biosensors, since being organic molecules they are incompatible, and less expensive. Therefore, biosensors based on the CISS effect could be manufactured to detect the virus that causes Covid-19 disease.

On the other hand, the CISS effect can allow the use of chiral molecules in the electrochemical process of hydrogen production, artificially, with greater efficiency. There are studies in which it is shown that, when the transfer of electrons is controlled in such a way that only one spin state is transferred, the efficiency improves significantly. Therefore, the CISS effect opens a new way to produce hydrogen more efficiently.

Another fascinating and important application of the CISS effect is in the pharmaceutical industry. Many drugs used for different ailments are made from chiral molecules, while one enantiomer produces relief, the other has different effects that, on the contrary, could be harmful. This is why the separation of the two components of chiral molecules is important in the process of making drugs, however, it is an expensive and different process for each type of molecule. Through the interaction of chiral molecules with a magnetic substrate and with the help of a magnet it is possible to separate the two types of molecules, allowing pharmacists to guarantee a drug with high purification with an easy and economical process. This method can also be used for other chemicals, such as pesticides.

# Bibliography

- [1] H.B.G. Casimir and R. Levensbericht. Kronig, in: Levensberichten en herdenkingen. pages 55–60, 1996.
- [2] P. Halpern. Spin: The quantum property that should have been impossible. <https://medium.com/starts-with-a-bang/spin-the-quantum-property-that-should-have-been-impossible-40bd52548b22>, 2017.
- [3] E. E. Fullerton and I. K. Schuller. The 2007 nobel prize in physics: Magnetism and transport at the nanoscale. *ACS Nano*, 1:384–389, 2007.
- [4] Hamelbeck V. Markus T. Z. Kettner M. Hanne G. F. Vager Z. Naaman R. Göhler, B. and H. Zacharias. Spin selectivity in electron transmission through self-assembled monolayers of double-stranded dna. *J. Sci.*, 331(6019):894–897, 2011.
- [5] Markus T. Cohen S. R. Vager Z. Gutierrez R. Xie, Z. and R. Naaman. Spin specific electron conduction through dna oligomers. *Nano Lett.*, 11(11):4652–4655, 2011.
- [6] Chapter 2: Nucleic acids and atp. <https://n9.cl/6kj0t>, 2010.
- [7] Mujica V. Varela, S. and E. Medina. Effective spin-orbit couplings in an analytical tight-binding model of dna: Spin filtering and chiral spin transport. *Phys. Rev. B*, 93, 2016.
- [8] Sanny J. Moebis W. Friedman G. Druger S. D. Kolakowska A. Anderson D. Bowman D. Demaree D. Ginsberg E. Ling, S. J. et al. University physics volume 3. 2018.
- [9] H. M. Pastawski and E. Medina. ‘tight binding’ methods in quantum transport through molecules and small devices: From the coherent to the decoherent description. *Rev. Mex. Fis.*, 47:1–23, Mar 2001.
- [10] C. Ertler P. Stano J. Fabian, A. Matos-Abiague and I. Zutic. Semiconductor spintronics. *acta physica slovacica. Reviews and Tutorials*, 57:565–907, 2007.
- [11] Fabian J. Žutić, I. and S. D. Sarma. Spintronics: Fundamentals and applications. *Rev. Mod. Phys.*, 76(2):323, 2004.
- [12] D. D. Awschalom and M. E. Flatté. Challenges for semiconductor spintronics. *Nature Physics*, 3:153–159, 2007.

- [13] S. A. Goudsmit. The discovery of the electron spin. *Foundations Of Modern Epr*, pages 1–12, 1998.
- [14] W. Gerlach and O. Stern. Der experimentelle nachweis der richtungsquantelung im magnetfeld. *Z. Phys.*, 9:349–352, 1922.
- [15] E. D. Commins. Electron spin and its history. *Annu. Rev. Nucl. Part. Sci.*, 62:133–157, 2012.
- [16] L. Bogani and W. Wernsdorfer. Molecular spintronics using single-molecule magnets. *J. Nanosci. Nanotechnol.*, pages 194–201, 2009.
- [17] S. Sanvito. Molecular spintronics. *Chem. Soc. Rev.*, 40:3336–3355, 2011.
- [18] A. Fert F. Nguyen Van Dau F. Petroff P. Eitenne G. Creuzet A. Friederich M. N. Baibich, J. M. Broto and J. Chazelas. Giant magnetoresistance of (001)fe/(001)cr magnetic superlattices. *Phys. Rev. Lett.*, 61:2472–2475, 1988.
- [19] F. Saurenbach G. Binasch, P. Grünberg and W. Zinn. Enhanced magnetoresistance in layered magnetic structures with antiferromagnetic interlayer exchange. *Phys. Rev. B*, 39:4828–4830, 1989.
- [20] S. Datta and B. Das. Electronic analog of the electro-optic modulator. *Appl. Phys. Lett.*, 56(7):665–667, 1990.
- [21] S. Chikuzami. *Physics of Ferromagnetism*. 1997.
- [22] D. Loss D. Awschalom and N. Samarth (ed.). *Semiconductor spintronics and quantum computation*. 2013.
- [23] Z. Valy Vardeny Z. H. Xiong, D. Wu and J. Shi. Giant magnetoresistance in organic spin-valves. *Nat.*, 427:821–824, 2011.
- [24] S. W. Bailey C. J. Lambert J. Ferrer A. R. Rocha, V. M. García-suárez and S. Sanvito. Towards molecular spintronics. *Nat. Mater.*, 4:335–339, 2005.
- [25] F. C. Maticcotta C. Taliani V. Dediu, M. Murgia and S. Barbanera. Room temperature spin polarized injection in organic semiconductor. *Solid State Commun.*, 122:181–184, 2002.
- [26] B. W. Alphenaar K. Tsukagoshi and H. Ago. Coherent transport of electron spin in a ferromagnetically contacted carbon nanotube. *Nat.*, 401:572–574, 1999.
- [27] M. Ouyang. Coherent spin transfer between molecularly bridged quantum dots. *Science*, 301:1074–1078, 2003.
- [28] M. S. Zöllner, S. Varela, E. Medina, V. Mujica, and C. Herrmann. Chiral-induced spin selectivity: A symmetry analysis of electronic transmission. *ChemRxiv*, 8325248:v1, 2019.
- [29] Yehuda B Band and Yshai Avishai. *Quantum mechanics with applications to nanotechnology and information science*. Academic Press, 2013.
- [30] G. Rikken and E. Raupach. Enantioselective magnetochiral photochemistry. *Nat.*, 405(6789):932–935, 2000.

- [31] S. Yeganeh, M. A. Ratner, E. Medina, and V. Mujica. Chiral electron transport: Scattering through helical potentials. *J. Chem. Phys.*, 131(1):014707, 2009.
- [32] R. Gutierrez, E. Díaz, R. Naaman, and G. Cuniberti. Spin-selective transport through helical molecular systems. *Phys. Rev. B*, 85(8):081404, 2012.
- [33] E. Medina, F. López, M. A. Ratner, and V. Mujica. Chiral molecular films as electron polarizers and polarization modulators. *EPL*, 99(1):17006, 2012.
- [34] B. K. Thomson and W. Thomson. *Baltimore lectures on molecular dynamics and the wave theory of light*. Cambridge University Press, 2010.
- [35] Georges H. Wagnière. *On chirality and the universal asymmetry: reflections on image and mirror image*. John Wiley & Sons, 2007.
- [36] Gutierrez R. Dianat A. Mujica V. Maslyuk, V. V. and Gianaurelio Cuniberti. Enhanced magnetoresistance in chiral molecular junctions. *J. Phys. Chem. Lett.*, 9(18):5453–5459, 2018.
- [37] Slater S. K. Petta, J.R. and D. C. Ralph. Spin-dependent transport in molecular tunnel junctions. *Phys. Rev. Lett.*, 93(13):136601, 2004.
- [38] A. Guo and Q. Sun. Spin-selective transport of electrons in dna double helix. *Phys. Rev. Lett.*, 108(21):218102, 2012.
- [39] Ananthavel S. P. Waldeck D. H. Ray, K. and R. Naaman. Asymmetric scattering of polarized electrons by organized organic films of chiral molecules. *J. Sci.*, 283(5403):814–816, 1999.
- [40] T. Aqua, R. Naaman, and S. S. Daube. Controlling the adsorption and reactivity of dna on gold. *Langmuir*, 19(25):10573–10580, 2003.
- [41] R Naaman and L Sanche. Low-energy electron transmission through thin-film molecular and biomolecular solids. *Chem. Rev.*, 107(5):1553–1579, 2007.
- [42] R Gutierrez, E Díaz, C Gaul, T Brumme, F Domínguez-Adame, and G Cuniberti. Modeling spin transport in helical fields: derivation of an effective low-dimensional hamiltonian. *J. Phys. Chem. C.*, 117(43):22276–22284, 2013.
- [43] A. Guo and Q. Sun. Spin-dependent electron transport in protein-like single-helical molecules. *Proc. Natl. Acad. Sci. U. S. A.*, 111(32):11658–11662, 2014.
- [44] J. Blumberger. Recent advances in the theory and molecular simulation of biological electron transfer reactions. *Chem. Rev.*, 115(20):11191–11238, 2015.
- [45] Santos T. S. Moodera, J. S. and T. Nagahama. The phenomena of spin-filter tunnelling. *J. Condens. Matter Phys.*, 19(16):165202, 2007.

- [46] Eugen Merzbacher. The early history of quantum tunneling. *Phys. Today*, 55(8):44–50, 2002.
- [47] J. J. Hopfield. Electron transfer between biological molecules by thermally activated tunneling. *Proc. Natl. Acad. Sci. U. S. A.*, 71(9):3640–3644, 1974.
- [48] Onuchic J. N. Beratan, D. N. and J. J. Hopfield. Electron tunneling through covalent and noncovalent pathways in proteins. *J. Chem. Phys.*, 86(8):4488–4498, 1987.
- [49] Dunn A. R. Hess C. R. Winkler, J. R. and H. B Gray. Electron tunneling through iron and copper proteins. In *Bioinorganic Electrochemistry*, pages 1–23. Springer, 2008.
- [50] Arkin M. R. Jenkins Y. Ghatlia N. D. Bossmann S. H. Turro N. J. Murphy, C. J. and J. K. Barton. Long-range photoinduced electron transfer through a dna helix. *J. Sci.*, 262(5136):1025–1029, 1993.
- [51] S. Varela. Transporte y polarización electrónica a través de películas quirales.
- [52] J. C. Slater and G. F. Koster. Simplified lcao method for the periodic potential problem. *Physical Review*, 94(6):1498, 1954.
- [53] J. M. Lia. Interacción espín-órbita en anillos cuánticos semiconductores delgados.
- [54] R. R. Sinden. *DNA structure and function*. Elsevier, 2012.
- [55] LGD Hawke, George Kalosakas, and Constantinos Simserides. Electronic parameters for charge transfer along dna. *Eur. Phys. J. E. Soft. Matter.*, 32(3):291, 2010.
- [56] T. Ando. Spin-orbit interaction in carbon nanotubes. *J. Phys. Soc. Jpn*, 69(6):1757–1763, 2000.
- [57] M. Razavy and J. G. Muga. Quantum theory of tunneling. *PhT*, 57(2):66–67, 2004.
- [58] M. Razavy. *Quantum theory of tunneling*. World Scientific, 2003.
- [59] E. Heifetz and I. Plohotnikov. Effective classical stochastic theory for quantum tunneling. *Phys. Lett. A.*, page 126511, 2020.
- [60] D. J. Griffiths. Introduction to quantum mechanics. 2nd, Pearson, Chapter2. *The time-independent schrodinger equation*, pages 24–92, 2005.
- [61] Dong-Kyun Seo. Spin polarization. *Handbook of Solid State Chemistry*, pages 261–283, 2017.
- [62] Bibes M. Bocher L. Valencia S. Kronast F. Crassous A. Moya X. Enouz-Vedrenne S. Gloter A. Imhoff D. Garcia, V. et al. Ferroelectric control of spin polarization. *Science*, 327(5969):1106–1110, 2010.
- [63] PS Farago. Electron spin polarization. *Rep. Prog. Phys.*, 34(3):1055, 1971.
- [64] D. T. Pierce. Spin-polarized electron microscopy. *Phys. Scr*, 38(2):291, 1988.

- [65] J. Unguris. 6. scanning electron microscopy with polarization analysis (sempa) and its applications. In *Experimental methods in the physical sciences*, volume 36, pages 167–XVI. Elsevier, 2001.
- [66] D. C. Worledge and T. H. Geballe. Maki analysis of spin-polarized tunneling in an oxide ferromagnet. *Phys. Review B*, 62(1):447, 2000.
- [67] E. M. Purcell. *Electricidad y magnetismo*, volume 2. Reverté, 1988.
- [68] D. Xiao J. Shi, P. Zhang and Q. Niu. Proper definition of spin current in spin-orbit coupled system. *Phys. Rev. B*, 96, 2006.
- [69] Daniel C Ralph and Mark D Stiles. Spin transfer torques. *J. Magn. Magn. Mater.*, 320(7):1190–1216, 2008.
- [70] H. M. Pastawski P. R. Levstein and J. L. D’Amato. Tuning the through-bond interaction in a two-centre problem. *J. Phys. Condens. Materia*, 2:1781–1794, 1990.
- [71] Montañes B. López F. Berche B. Guillot B. Mujica V. Varela, S. and E. Medina. Intrinsic rashba coupling due to hydrogen bonding in dna. *J. Chem. Phys.*, 151(12):125102, 2019.
- [72] R. Winkler. Spin-orbit coupling effect in two-dimensional electron and hole systems. *Springer Verlag GmbH*, 2003.
- [73] González-Arraga L. A. Finkelstein-Shapiro D. Berche B. Medina, E. and V. Mujica. Continuum model for chiral induced spin selectivity in helical molecules. *J. Chem. Phys.*, 142(19):194308, 2015.
- [74] Nordholm S. Cribb, P. H. and N. S. Hush. A density matrix approach to double well transfer: effects of asymmetry on the tunneling rate. *Chem. Phys.*, 44(3):315–335, 1979.
- [75] K. L. Davis-S. Bezer J. Kong Y. Xing E. Borguet-C. Achim D. N. Beratan E. Wierzbinski, R. Venkatramani and D. H. Waldeck. The single-molecule conductance and electrochemical electron-transfer rate are related by a power law. *ACS Nano*, 2013.
- [76] K. Michaeli and R. Naaman. Origin of spin-dependent tunneling through chiral molecules. *J. Chem. Phys.*, 123:17043–17048, 2019.
- [77] R. Gutierrez N. V. Grib, D. A. Ryndyk and G. Cuniberti. Distance-dependent coherent charge transport in dna: crossover from tunneling to free propagation. *J. Biophys. Chem.*, 1:77–85, 2010.
- [78] S. Varela, V. Mujica, and E. Medina. Spin-orbit coupling modulation in dna by mechanical deformations. *CHIMIA*, 72:411–417(7), 2018.
- [79] Korytár R. Sukenik N. Vardimon R. Kumar B. Nuckolls C. Evers F. Yelin, T. and O. Tal. Conductance saturation in a series of highly transmitting molecular junctions. *Nat. Mater.*, 15(4):444–449, 2016.
- [80] Gutierrez R. Mujica V. Geyer, M. and G. Cuniberti. Chirality-induced spin selectivity in a coarse-grained tight-binding model for helicene. *J. Phys. Chem. C.*, 123(44):27230–27241, 2019.



# Abbreviations

**CISS** Chiral Induced Spin Selectivity vii, 4–7

**DOS** density of states 18

**GMR** Giant Magneto-Resistance 2

**ISO** Intrinsic Spin-Orbit vii, xii, 5–7, 10, 11, 13, 14, 19, 31, 42

**LCAO** linear combination of atomic orbitals 22

**SEMPA** Scanning Electron Microscopy with Polarization Analysis 18

**SO** Spin-Orbit xii, xiii, 13, 25, 27, 34–37, 43–45

**STM** Scanning Tunneling Microscope 15, 18